Electrical Power and Energy Systems 105 (2019) 249–271

Contents lists available at ScienceDirect

Electrical Power and Energy Systems

journal homepage: www.elsevier.com/locate/ijepes

Constrained population extremal optimization-based robust load frequency control of multi-area interconnected power system

Kangdi Lu[a], Wuneng Zhou[a,*], Guoqiang Zeng[b,*], Yiyuan Zheng[c]

[a] Department of Automation, College of Information Sciences and Technology, Donghua University, Shanghai 201620, China
[b] National-Local Joint Engineering Laboratory of Digitalize Electrical Design Technology, Wenzhou University, Wenzhou 325035, China
[c] Wenlan School of Business, Zhongnan University of Economics and Law, Wuhan 430073, China

ARTICLE INFO

Keywords:
Load frequency control
Robust PI controller
Constrained evolutionary optimization
Population extremal optimization
Multi-area interconnected power system

ABSTRACT

This paper proposes a robust proportional-integral (PI) controller with its parameters designed by constrained population extremal optimization for load frequency control problem of multi-area interconnected. During the process of optimization, the robust performance index is used as fitness function, where linear matrix inequalities technique is employed to describe the H_∞ constraint, and the taking error performance requirement such as integral time absolute error is incorporated as another constraint. Three different two-area interconnected power systems are used as test systems to demonstrate the effectiveness of the proposed controller by comparing with other PI control methods and one optimized model predictive control. In addition, in order to investigate the performance of proposed controller for the LFC problem of large scale system, a three-area interconnected power system is used as another test system. The comprehensive experimental results fully demonstrate that the proposed control scheme in this paper performs better than other control strategies on the most considered scenarios under the conditions of load disturbance and parameters uncertainties in terms of system response and control performance indices.

1. Introduction

Load frequency control (LFC) is of great importance for power systems or microgrids to maintain the scheduled system frequency and power exchange between areas during normal and abnormal conditions [1]. The control objective of LFC is to minimize the frequency deviation and net tie-line flow error between control areas. More specifically, the LFC should be ensured stabilization considering system nonlinearities, model parameters uncertainties, and load disturbance or resonance attack [1–4], which may take place in realistic power engineering. Over the past decades, considerable efforts have been devoted to developing control strategies for LFC problem, which can be roughly separated into two categories. The first category employs various advanced techniques [4–14] to design advanced controllers for LFC of interconnected power system or microgrids. For example, model predictive control [6–9], H_∞ and μ-synthesis [10], fuzzy logic [12,13] and sliding model technique [14] have been utilized for LFC issue. The second category is known as proportional-integral-derivative (PID) [15,16] or proportional-integral (PI) controller [17–28], which keeps preferred choice of an engineer because of the simple but reliable control structure. Also, the PI/PID controller needs lower user-skill requirements and offers simplified dynamic model, so it is favorable in engineering practice. Thanks to these attractive properties, the control strategies of LFC system equipped with PI controller have witnessed a boom of development since last two decades [17–28] Ali et al. [17] applied the bacteria foraging optimization to deal with LFC problem of two-area interconnected power system. Mohanty et al. [18] used differential evolution (DE) algorithm to design PI controller for LFC considering multi-source in power system. In [20,21], the authors used cuckoo search (CS) algorithm and bat algorithm to solve the LFC problem considering some nonlinear terms e.g., generation rate constraint (GRC) and governor dead band (GDB). Adb-Elazim et al. [22] designed the load frequency controller of two-area system via firefly algorithm. In [23,24], authors suggested PI controllers equipped with fuzzy systems for LFC problems. Rerkpreedapong et al. [26] suggested genetic algorithm (GA) to tune the PI control parameters subjecting to the H_∞ constraints in terms of LMI. In addition, Pandey et al. [28] combined the particle swarm optimization (PSO) and linear matrix inequalities (LMI) to design robust PI controller for LFC in hybrid power systems. As mentioned above, the control methods in [26,28] based on LMI technique, but these methods do not take into account some nonlinear features simultaneously. From a comprehensive literature survey on the LFC

* Corresponding authors.
E-mail addresses: zhouwuneng@163.com (W. Zhou), zeng.guoqiang5@gmail.com (G. Zeng).

https://doi.org/10.1016/j.ijepes.2018.08.043
Received 5 April 2018; Received in revised form 6 August 2018; Accepted 23 August 2018

Nomenclature

i	the subscript referring to i-th area
Δ	deviation
f	the system frequency
ACE_i	area control error
N	the number of areas
λ_i	frequency bias parameter
D_i	generator damping coefficient
R_i	speed regulation
T_{gi}	the speed governor time constant
T_{ti}	the turbine time constant
T_{ri}	the reheat time constant
K_{ri}	The p.u megawatt rating of high pressure stage
J	objective function
u_i	controller output signal
T_w	The hydro turbine time constant
K_{pi}, T_{pi}	The time constant and gain of power system
ΔP_{tiei}	tie-line flow error
K_{PP}, K_{II}	the parameters of PI controller
t	time in second
T_{ij}	tie-line synchronizing coefficient between area i and j
ΔP_{Li}	load disturbance
t_{sim}	time range of simulation

List of abbreviations

LFC	load frequency control
(C)PEO	(constrained) population extremal optimization
LMI	linear matrix inequalities
PI	proportional-integral
PID	proportional-integral-derivative
GA	genetic algorithm
(C)PSO	(constrained) particle swarm optimization
BFOA	bacterial foraging optimization algorithm
MPC	model predictive control
ACO	ant colony optimization
ABC	artificial bee colony
GRC	generation rate constraint
GDB	governor dead band
IAE	Integral of absolute error
ISE	Integral of square error
ITAE	Integral of time multiplied absolute error
ITSE	Integral of time multiplied square error

issues of power systems presented in [1], few works focus on LMI technique subject to the H_∞ constraint for the LFC issue by considering these characteristics of realistic power system simultaneously.

As reported in [29–31], in presence of time delays or nonlinearities such as GRC and GDB, most existing LFC methodologies exhibit relative poor control performance. To the best of our knowledge, only few research works consider a multi-area interconnected power system with these severe and realistic factors. Elsisi et al. [30] proposed a novel model predictive control method optimized by bat inspired algorithm (BIA-MPC) for LFC of a two-area hydro-thermal power including GRC, GDB, time delays and thermodynamic process, and its effectiveness is illustrated by comparing with GA-based PI controller and conventional PI control method. However, as advanced controller, BIA-MPC is more complex than PI-type controller, from an implementation point of view. By considering these nonlinear features, it is still a tremendously challenge to improve LFC performance by PI-type controller especially suffering from load fluctuations and parameters uncertainty. As discussed in [20,21], the evolutionary algorithm techniques-based PI controllers have potential ability to handle nonlinear terms by minimizing the integral time absolute error (*ITAE*) performance index. In addition, as discussed in [32], a tracking error performance requirement constraint i.e., *ITAE*, which is used to obtain the desired performance, contributes to improving the control performance for various systems (e.g., pneumatic servo system, separating tower process and F18 fighter aircraft system). On the other hand, for improving the control system performance, using H_∞ performance or taking error performance as fitness function is often not enough [33]. Thus, combining the performance requirement constraint i.e., *ITAE* with H_∞ performance described by LMI technique may improve LFC performance to some extent.

Recently, in evolutionary computing literature, extremal optimization (EO) [34,35], provides a novel insight due to its heuristic mechanism from self-organized criticality [36]. EO abandons elite selection mechanism while focuses on changing the bad elements or individuals by mutation. As a result, EO and its variations such as population extremal optimization (PEO) [37] and multi-objective population-based extremal optimization (MOPEO) [38,39], have been widely applied by many researchers in combinatorial and continuous optimization domain [40–45] Also, EO and its variations have been demonstrated more efficient because of their advantages in computational complexity, memory requirements and adjustable parameters compared to other popular nature-inspired algorithms including GA and PSO. Unfortunately, there are only few reported works concerning constrained population extremal optimization (CPEO), let alone concerning CPEO-based LMI technique subjecting to the H_∞ constraint and performance requirement constraint in optimal design of PI controller for multi-area power system. This is one of primary motivations to extend PEO algorithm to the constrained version by embedded into tournament-constraint-handling method [46] for designing robust PI controller for LFC of power system.

Motivated by the analysis above, this paper proposes a robust PI control scheme called CPEO-LMI-PI with its control parameters designed by CPEO wherein the LMI technique is employed to describe the H_∞ constraint, and the *ITAE* performance is incorporated as another constraint. Compared with existing controllers by minimizing the robust performance index, the proposed control scheme in this paper has following advantages:

(1) The H_∞-LMI control strategy has disadvantage in structure controller which is high order and inapplicable to implement, while the proposed CPEO-LMI-PI is a PI-type which is more appealing from an implementation point of view.
(2) The control methods reported in [26,28] ignore some nonlinear terms e.g., GRC and GDB, while the proposed controller considers these nonlinear terms by solving a constraint i.e., *ITAE* performance index during the simulation.
(3) Although there are many popular evolutionary algorithm techniques such as GA and PSO, these algorithms may pain from slow convergence and may get local minimum solutions. As for PEO algorithm with less adjustable parameters, the optimization ability has been demonstrated by various problems. Thus, to solve the

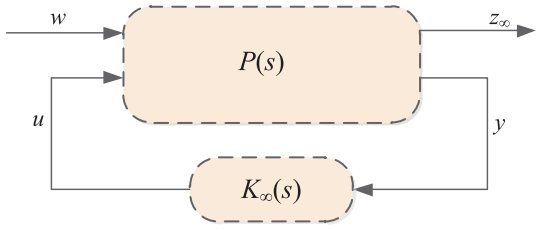

Fig. 1. The block diagram of closed-loop system via robust H_∞ control.

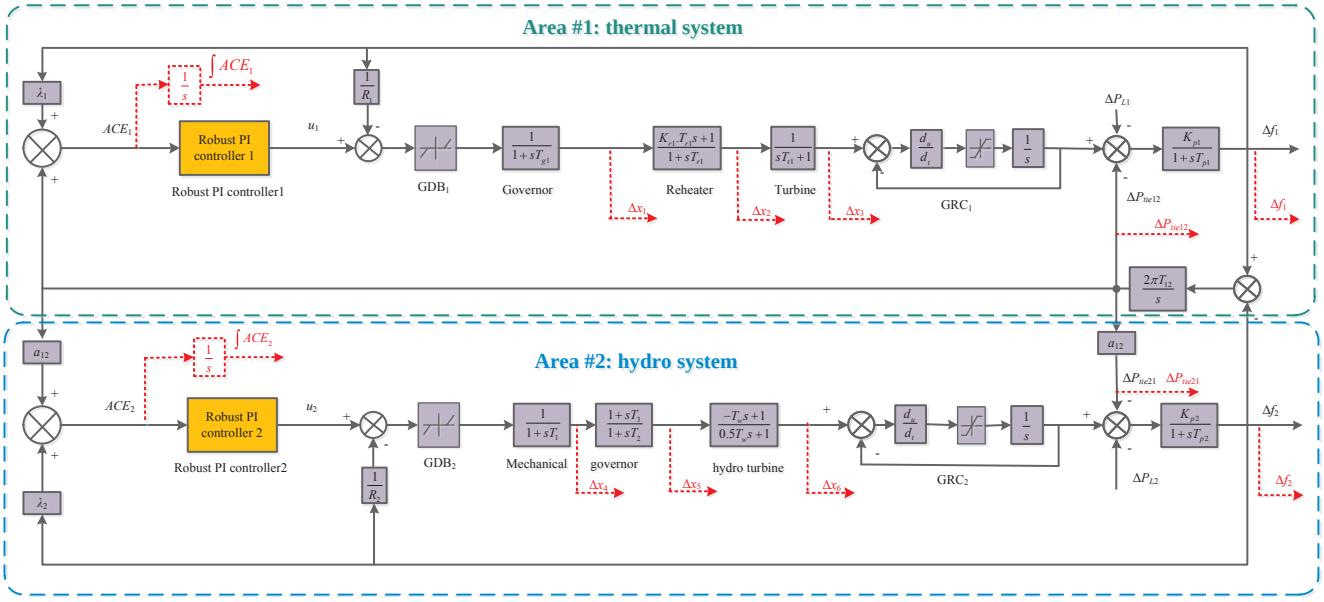

Fig. 2. The schematic diagram of two-area interconnected power system with GRC and GDB.

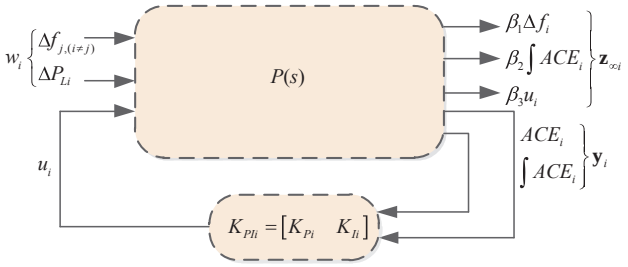

Fig. 3. Robust PI control framework.

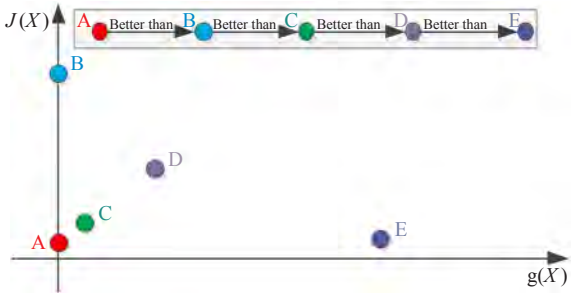

Fig. 4. The tournament-constraint-handling (THC) rule.

constrained optimization problem, the CPEO has advantage in global search ability and less control parameters.

Compared with CPSO-LMI-PI controller and other existing controllers on four different interconnected power systems, the proposed control scheme in this paper will be validated to be better in terms of system response and control performance indices. Our contributions of this study are summarized as follows:

(1) We extend the traditional PEO algorithm to solve a constrained problem by embedding into the tournament-constraint-handling method.
(2) The LFC problem is formulated as a constrained problem and the proposed CPEO-LMI-PI controller is designed by a CPEO, based on LMI technique subjecting to the H_∞ constraints and a taking error performance requirement as another constraint.
(3) Compared with CPSO-LMI-PI controller, the proposed CPEO-LMI-PI converges faster, obtains smaller objective function value, and better control performance under various loading scenarios suffering from system nonlinearities.
(4) The proposed CPEO-LMI-PI control strategy can be considered as a novel PI-type controller to improve the control performance by comparing with some existing control methods.

The rest of this paper is organized as follows. Section 2 introduces preliminaries concerning on LMI based H_∞ control theory, and an example of dynamical model for two-area interconnected power system. Then, the proposed CPEO-LMI-PI control scheme is described in detail in Section 3. The comprehensive experimental results are given and analyzed in Section 4. Finally, we draw the conclusion and thread some future research issues in Section 5.

2. Technical background

In this section, a brief overview of LMI based H_∞ control technique is given. Then, we give an example of the dynamic model for a two-area interconnected power system.

2.1. LMI-based h_∞ control technique

A classical closed-loop structure of robust control problem is represented in Fig. 1 [26,28], where w, z_∞, u, y represent the disturbance, control variable, control law, measured variable, respectively. The $P(s)$ and $K_\infty(s)$ denote a linear-invariant system and a robust H_∞ controller, respectively. And the state space realization of system model and controller are given by formula (1) and formula (2), respectively.

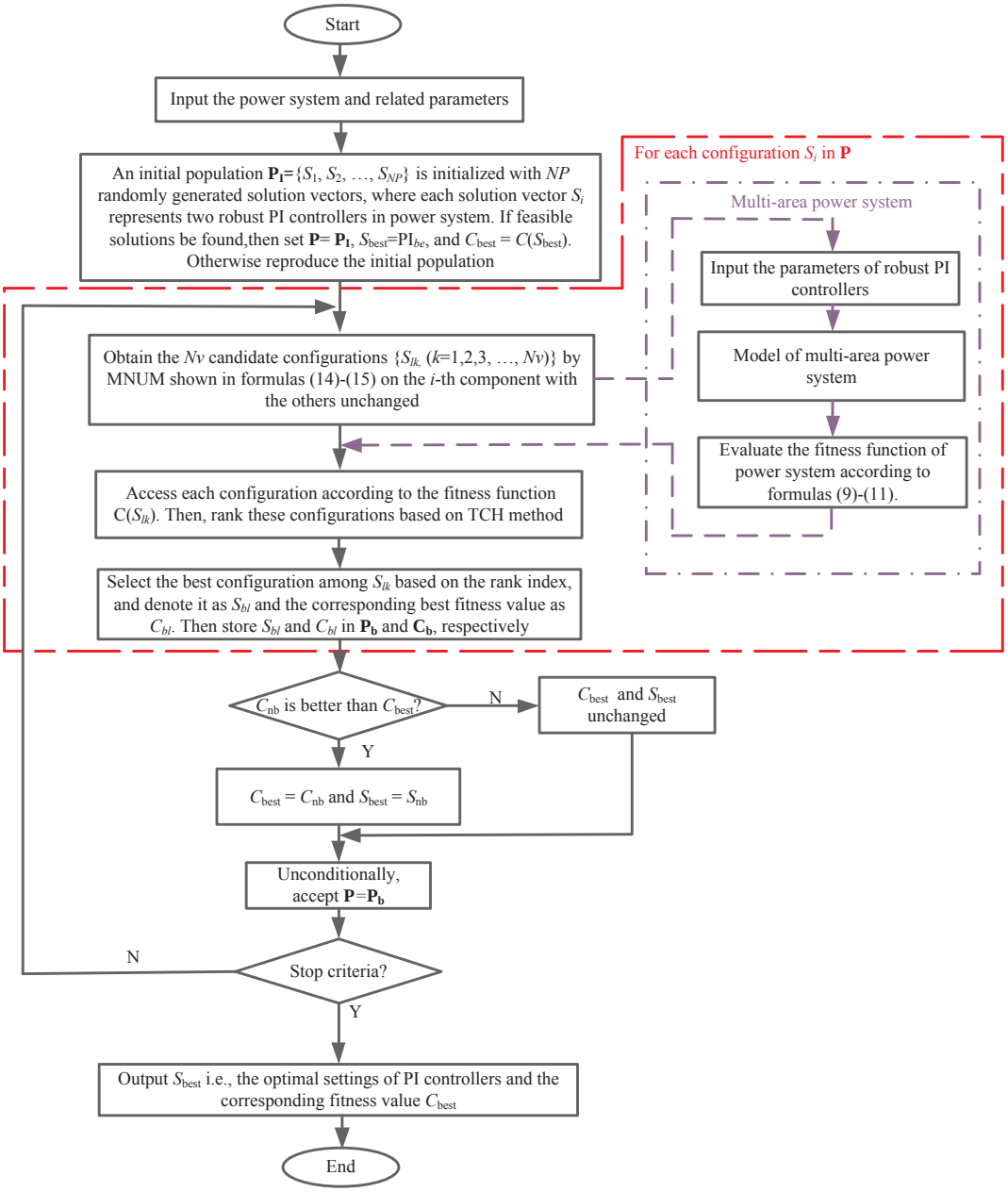

Fig. 5. The flowchart of the proposed CPEO-LMI-PI control scheme.

Table 1
The main difference of four Experiments.

Experiment	Scale of power system	Characteristics	Competitors
Experiment I	Two-areas	GRC, GDB	CPSO-LMI-PI
Experiment II	Two-areas	Linear	BFOA-PI [17], GA-PI [17], conventional PI [17]
Experiment III	Two-areas	GRC, GDB, boiler dynamics and constant time delay	GA-PI [30], conventional PI [30], BIA-MPC [30]
Experiment IV	Three-areas	Rate limiter	H_∞-LMI controller [26]

$$\begin{cases} \dot{x} = Ax + B_1 w + B_2 u \\ z_\infty = C_1 x + D_{11} w + D_{12} u \\ y = C_2 x + D_{21} w \end{cases} \quad (1)$$

$$\begin{cases} \dot{\xi}_\infty = A_{k\infty}\xi_\infty + B_{k\infty} y \\ u = C_{k\infty}\xi_\infty + D_{k\infty} y \end{cases} \quad (2)$$

where ξ_∞ is the state vector for H_∞ controller. Combining formula (1) and formula (2), the closed-loop system is obtained as formula (3):

$$\begin{cases} \dot{x}_{cl} = A_{cl} x_{cl} + B_{cl} w \\ z_\infty = C_{cl} x_{cl} + D_{cl} w \end{cases} \quad (3)$$

Table 2
The parameters of PSO-LMI-PI and CPEO-LMI-PI used in the experiments.

Algorithm	Parameters	Number of parameters	Controller
CPSO-LMI-PI	Population (swarm) size $NP = 40$, The maximum number of iterations $I_{max} = 100$, inertia weight $w_{max} = 0.6$, the acceleration factors $c_1 = 1.0$, $c_2 = 1.0$, the limits of velocity $V_{max} = 0.5$, $V_{min} = -0.5$, the lower and upper of PI parameters $\mathbf{L} = -2$ $\mathbf{U} = 10$; performance requirement P_D	10	Controller of area 1: $G_{PI_1} = -1.4091 + \frac{-0.9907}{s}$ Controller of area 2: $G_{PI_2} = 0.4164 + \frac{-0.1344}{s}$
CPEO-LMI-PI	Population size $NP = 10$, maximum number of iterations $I_{max} = 100$, parameter $b = 3$ used in MNUM operation, the lower and upper of PI parameters $\mathbf{L} = -2$ $\mathbf{U} = 10$. performance requirement P_D	6	Controller of area 1: $G_{PI_1} = -1.8066 + \frac{-0.7005}{s}$ Controller of area 2: $G_{PI_2} = 0.3785 + \frac{-0.0896}{s}$

Table 3
Best objective function value J and the convergent generations.

Control method	Best objective function value (J)	Convergent generations
CPSO-LMI-PI	$J = 311.24$	62
CPEO-LMI-PI	$J = 300.81$	49

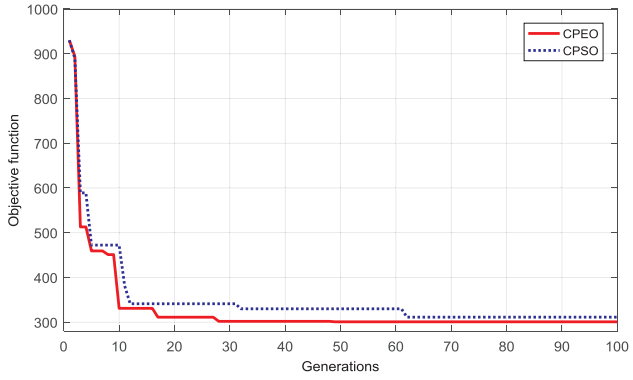

Fig. 6. Comparison of convergence process of best objective function value obtained by CPEO and CPSO.

Table 4
The conditions of test scenarios on Experiment I.

Scenarios	Condition
Scenario1	The second area undergoes 0.05 step increase in demand i.e., $\Delta P_{L2} = 0.05$ p.u.
Scenario 2	The first area and second area simultaneously undergo 0.05 step increase in demand, $\Delta P_{L1} = 0.05$p.u, $\Delta P_{L2} = 0.05$ p.u.
Scenario 3	Parameter T_g increase and decrease 50% under $\Delta P_{L2} = 0.05$ p.u.
Scenario 4	Parameter T_{12} increase and decrease 50% under $\Delta P_{L2} = 0.05$ p.u.
Scenario 5	The first area and second area simultaneously undergo dynamical fluctuations of ΔP_{L1}, ΔP_{L2}.

$$\text{where} \quad x_{cl} = \begin{bmatrix} x \\ \xi_\infty \end{bmatrix}, \; A_{cl} = \begin{bmatrix} A + B_2 D_{k\infty} C_2 & B_2 C_{k\infty} \\ B_{k\infty} C_2 & A_{k\infty} \end{bmatrix}, \; B_{cl} = \begin{bmatrix} B_1 + B_2 C_{k\infty} D_{21} \\ B_{k\infty} D_{21} \end{bmatrix}, \; C_{cl} = [C_1 + D_{12} D_{k\infty} C_2 \quad D_{12} C_{k\infty}], \; D_{cl} = [D_{11} + D_{12} D_{k\infty} D_{21}].$$

On the basis message of y (measured variable), the H_∞ control technique aims at designing an optimal control value u (control law) so that the value of w (the disturbance) on z_∞ (control variable), which is expressed by the infinity norm $||T_{z_\infty w}||_\infty$ ($T_{z_\infty w}$ is the transfer function from z_∞ to w), does not surpass a specified positive number γ in order to assure robust performance. According to the following lemma [47], the H_∞ control design can be formulated in terms of LMI.

Lemma ([47]). *The closed-loop RMS (root-mean-square) gain from z_∞ to w does not exceed γ, if and only if there exists a symmetric matrix X_∞ such that*

$$\begin{bmatrix} A_{cl} X_\infty + X_\infty A_{cl}^T & B_{cl} & X_\infty C_{cl}^T \\ B_{cl}^T & -I & D_{cl}^T \\ C_{cl} X_\infty & D_{cl} & -\gamma^2 I \end{bmatrix} < 0 \qquad X_\infty > 0 \tag{4}$$

Then, an optimal H_∞ control design can be achieved by minimizing the performance index γ subject to the above matrix inequalities.

2.2. An example of system dynamic model

The schematic diagram of two-area interconnected power system is shown in Fig. 2, where the two areas are incorporated with GRC and GDB. Note that the control objective of LFC is the area control error (ACE), shown in formula (5), which consists of frequency deviation (Δf) and net tie-line flow error (ΔP_{tie}).

$$ACE_i = \Delta P_{tie,i} + \lambda_i \Delta f_i, \; i = 1, 2. \tag{5}$$

where the λ_i is the frequency bias factor of i-th area.

To design the H_∞ controller based LMI, the state space model is given as follows.

$$\begin{cases} \dot{\mathbf{x}}_i = A_i \mathbf{x}_i + B_{1i} \mathbf{w}_i + B_{2i} \mathbf{u}_i \\ \mathbf{z}_{i\infty} = C_{1i} \mathbf{x}_i + D_i \mathbf{u}_i \\ \mathbf{y}_i = C_{2i} \mathbf{x}_i \end{cases} \tag{6}$$

For thermal area, the state variable (i.e., the red dotted line of thermal system in Fig. 2) is developed as:

$$\mathbf{x}_1 = [\Delta f_1 \quad \Delta P_{tie12} \quad \int ACE_1 \quad \Delta x_1 \quad \Delta x_2 \quad \Delta x_3]^T, \; \mathbf{w}_1 = [\Delta P_{L1} \quad \Delta f_2]^T, \; \mathbf{u}_1 = u_1,$$

$$\mathbf{z}_{1\infty} = [\beta_1 \Delta f_1 \quad \beta_2 \int ACE_1 \quad \beta_3 u_1]^T, \; \mathbf{y}_1 = [ACE_1 \quad \int ACE_1]^T.$$

$$A_1 = \begin{bmatrix} -\frac{1}{T_p} & -\frac{K_p}{T_p} & 0 & 0 & 0 & \frac{K_p}{T_p} \\ 2\pi T_{12} & 0 & 0 & 0 & 0 & 0 \\ \lambda_1 & 1 & 0 & 0 & 0 & 0 \\ -\frac{1}{T_g * R_1} & 0 & 0 & -\frac{1}{T_g} & 0 & 0 \\ -\frac{Kr}{T_g * R_1} & 0 & 0 & \frac{1}{T_r} & -\frac{K_r}{T_g} & -\frac{1}{T_r} \\ 0 & 0 & 0 & 0 & \frac{1}{T_t} & -\frac{1}{T_t} \end{bmatrix}, \; B_{11} = \begin{bmatrix} 0 & -\frac{K_p}{T_p} \\ -2\pi T_{12} & 0 \\ 0 & 0 \\ 0 & 0 \\ 0 & 0 \\ 0 & 0 \end{bmatrix}, \; B_{21} = \begin{bmatrix} 0 \\ 0 \\ 0 \\ \frac{1}{T_g} \\ \frac{K_r}{T_g} \\ 0 \end{bmatrix}, \; C_{11} = \begin{bmatrix} \beta_1 & 0 & 0 & 0 & 0 & 0 \\ 0 & 0 & \beta_2 & 0 & 0 & 0 \\ 0 & 0 & 0 & 0 & 0 & 0 \end{bmatrix},$$

$$D_1 = \begin{bmatrix} 0 \\ 0 \\ \beta_3 \end{bmatrix},$$

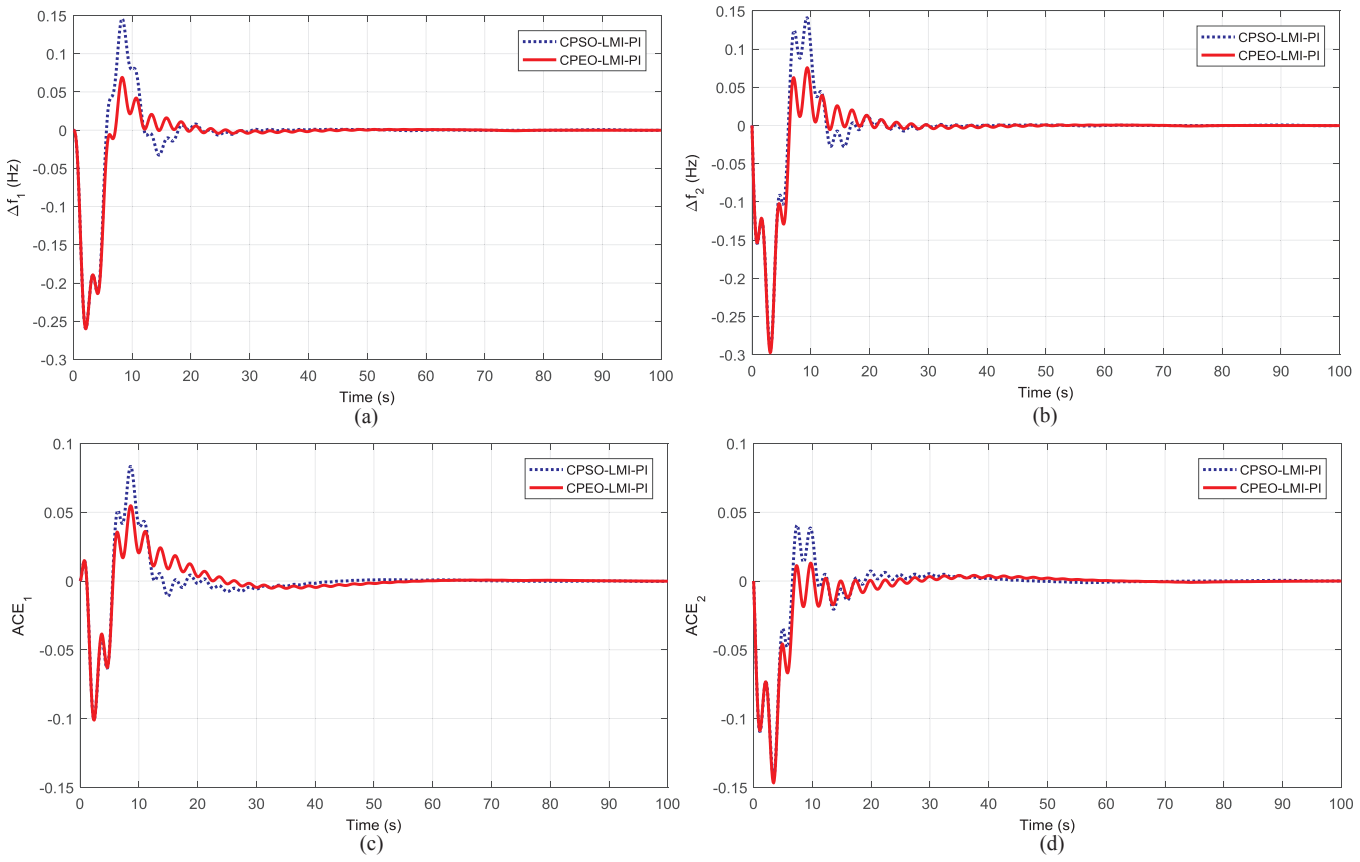

Fig. 7. Comparison of system response subject to Scenario 1 under Experiment I: (a) Δf_1, (b) Δf_2, (c) ACE_1 deviation (d) ACE_2 deviation.

Table 5
Performance comparison of CPSO-LMI-PI and CPEO-LMI-PI for Scenario 1 under Experiment I.

Algorithm	*IAE*	*ITAE*	*ISE*	*ITSE*
CPSO-LMI-PI	3.4405	26.9868	0.44939	1.9487
CPEO-LMI-PI	2.9584	23.7977	0.38367	1.3268

For hydro area, the state variable (i.e., the red dotted line of hydro system in Fig. 2) is developed as:

$$\mathbf{x}_2 = [\Delta f_2 \quad \Delta P_{tie21} \quad \int ACE_2 \quad \Delta x_4 \quad \Delta x_5 \quad \Delta x_6]^T, \mathbf{w}_2 = [\Delta P_{L2} \quad \Delta f_1]^T, \mathbf{u}_2 = u_2,$$

$$\mathbf{z}_{2\infty} = [\beta_1 \Delta f_2 \quad \beta_2 \int ACE_2 \quad \beta_3 u_2]^T, \ \mathbf{y}_2 = [ACE_2 \quad \int ACE_2]^T.$$

$$A_2 = \begin{bmatrix} -\frac{1}{T_{p_2}} & \frac{K_{p_2}}{T_{p_2}} & 0 & 0 & 0 & \frac{K_{p_2}}{T_{p_2}} \\ -2\pi T_{12} & 0 & 0 & 0 & 0 & 0 \\ \lambda_2 & -1 & 0 & 0 & 0 & 0 \\ -\frac{1}{T_1 * R_2} & 0 & 0 & -\frac{1}{T_1} & 0 & 0 \\ -\frac{T_2}{T_3 R_2 T_1} & 0 & 0 & \frac{1}{T_3} - \frac{T_2}{T_3 T_1} & -\frac{1}{T_3} & 0 \\ \frac{2T_2}{T_3 R_2 T_1} & 0 & 0 & \frac{-2}{T_3} + \frac{2T_2}{T_3 T_1} & \frac{2}{T_w} + \frac{2}{T_3} & -\frac{2}{T_w} \end{bmatrix}, \quad B_{12}$$

$$= \begin{bmatrix} 0 & -\frac{K_{p_2}}{T_{p_2}} \\ 2\pi T_{12} & 0 \\ 0 & 0 \\ 0 & 0 \\ 0 & 0 \\ 0 & 0 \end{bmatrix}, \quad B_{22} = \begin{bmatrix} 0 \\ 0 \\ 0 \\ \frac{1}{T_1} \\ \frac{T_2}{T_3 T_1} \\ -\frac{2T_2}{T_3 T_1} \end{bmatrix}, \quad C_{12} = \begin{bmatrix} \beta_1 & 0 & 0 & 0 & 0 & 0 \\ 0 & 0 & \beta_2 & 0 & 0 & 0 \\ 0 & 0 & 0 & 0 & 0 & 0 \end{bmatrix},$$

$$D_2 = \begin{bmatrix} 0 \\ 0 \\ \beta_3 \end{bmatrix}, C_{22} = \begin{bmatrix} \lambda_2 & 1 & 0 & 0 & 0 & 0 \\ 0 & 0 & 1 & 0 & 0 & 0 \end{bmatrix}$$

where β1, β2, β3 are the weighting coefficients which should be chosen by the designer for achieving the desired control performance.

The typical H_∞ controller, whose structure is a high order model, is not suitable for LFC problem in practice. Here, H_∞ controller is transformed to a PI-type controller according to the robust performance index γ [26]. The ACE is used as input signal and the formula is described as follow:

$$u_i = \Delta P_{Ci} = K_{Pi} ACE_i + K_{Ii} \int ACE_i = [K_{PPi} \quad K_{IIi}] \begin{bmatrix} ACE_i \\ \int ACE_i \end{bmatrix} = K_{PIi} y_i \tag{7}$$

Next, formula (7) is substituted into formula (6). Then, the close-loop system can be obtained as follow:

$$\begin{cases} \mathbf{u}_i = K_{PIi} C_2 \mathbf{x}_i \\ \dot{\mathbf{x}}_i = A_{cl} \mathbf{x}_i + B_{cl} \mathbf{w}_i \\ \mathbf{z}_{i\infty} = C_{cl} \mathbf{x}_i + D_{cl} \mathbf{w}_i \end{cases} \tag{8}$$

where $A_{cl} = A_i + B_{2i} K_{PIi} C_{2i}$, $B_{cl} = B_{1i}$, $C_{cl} = C_{1i} + D_i K_{PIi} C_{2i}$, $D_{cl} = \mathbf{0}$.

The corresponding control framework is shown in Fig. 3.

Remark 1. The dynamic model of system can be extended to a large scale system. For example, to deal with LFC of a three-area interconnected power system, we can develop the state variable of the third area. Then, we can get the corresponding matrix in formula (6). Finally, the form of formula (8) can be obtained to describe the third area. Similar operation can be done for larger scale power system.

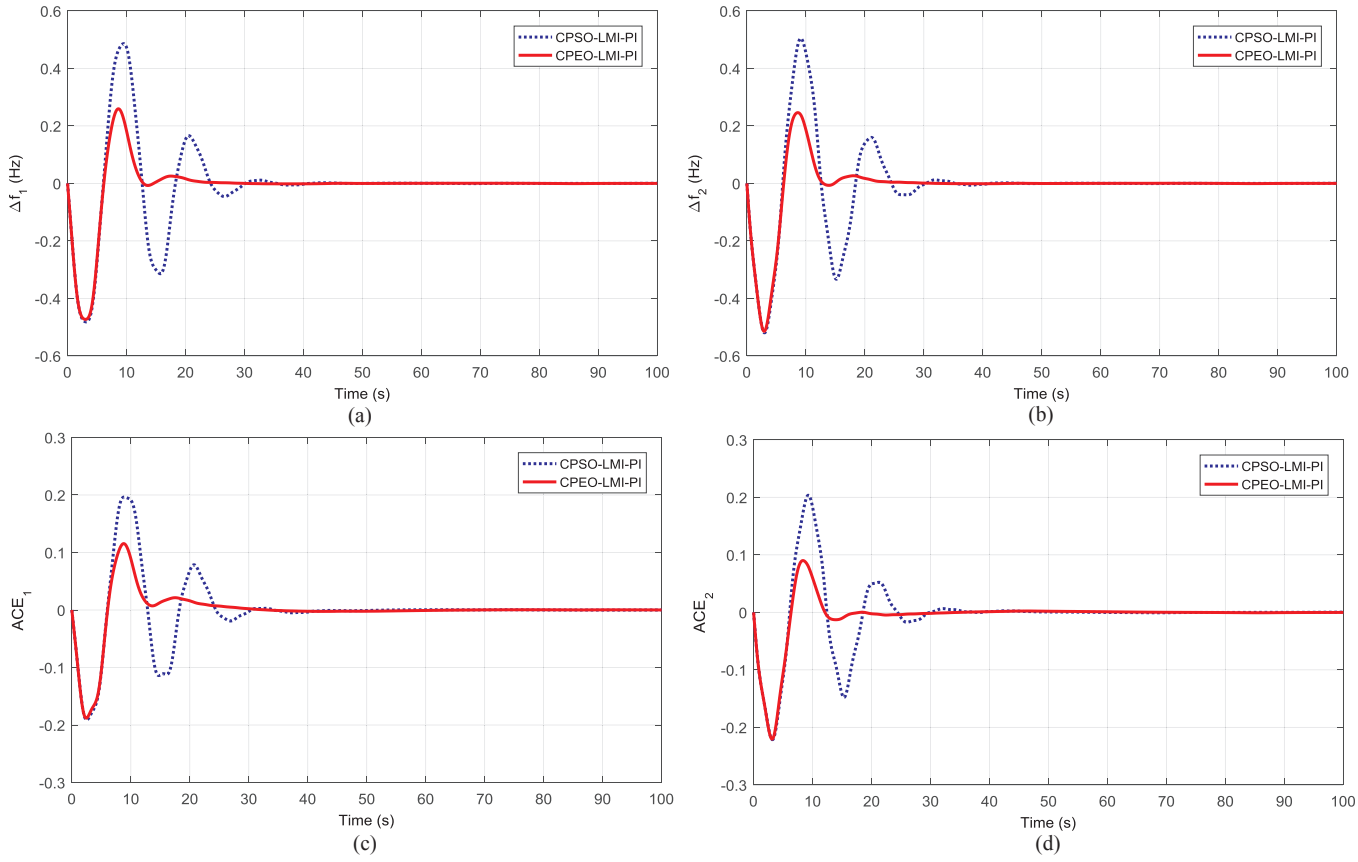

Fig. 8. Comparison of system response subject to Scenario 2 under Experiment I: (a)Δf_1, (b) Δf_2, (c) ACE_1 deviation (d) ACE_2 deviation.

Table 6
Performance comparison of CPSO-LMI-PI and CPEO-LMI-PI for Scenario 2 under Experiment I.

Algorithm	*IAE*	*ITAE*	*ISE*	*ITSE*
CPSO-LMI-PI	12.3399	131.4161	3.9212	32.30183
CPEO-LMI-PI	6.4322	44.31093	1.8653	7.8126

Remark 2. As reported in [20,21], ITAE performance index by the application of evolutionary algorithm techniques can handle the nonlinear terms to a certain extent. In addition, as reported in [26], the nonlinear terms are ignored when designing the state space model but these terms can be considered during the simulation. In this paper, the nonlinear terms are also ignored in the state space model, but the proposed ITAE performance requirement with CPEO algorithm can consider and copy with these factors during the simulation process.

3. The proposed control scheme

This section introduces the CPEO-LMI-PI control design method. Firstly, candidate objective function is chosen in Section 3.1. Then, main mechanism of the proposed control scheme is described in the Section 3.2. Finally, the analysis of CPEO-LMI-PI control scheme is given in the Section 3.3.

3.1. Candidate objective function

As mentioned previously, the power system suffers from nonlinearities such as GRC, GDB shown in Fig. 2 and the corresponding system parameters, GRC, and GDB are listed in Appendix A.1. In order to obtain high-quality control performance, the controller has to deal with these nonlinearities which cause relative poor dynamic performance [29,30].Unfortunately, in most of previous reported works [26,28], only robust performance index γ is adopted as objective function based LMI subject to H_∞ constraints (mentioned in Section 2.1), which is not enough to handle these nonlinearities and get satisfied control performance. Also, the eigenvalue-based fitness definition described in [48] is not suitable due to these nonlinearities. Consequently, this paper suggests another constraint, *ITAE* taking error performance requirement, incorporated into objective function during the optimization process. Accordingly, the design optimization problem can be described as follows:

$$\text{Consider } X = [K_{PP1},\ K_{II1},\ K_{PP2},\ K_{II2},\ ...,\ K_{PPN},\ K_{IIN}]$$

$$\text{Minimize } J(X) = \sum_{i=1}^{N} \gamma_i \tag{9}$$

$$Subject\ to \begin{cases} \begin{bmatrix} A_{cl}X_\infty + X_\infty A_{cl}^T & B_{cl} & X_\infty C_{cl}^T \\ B_{cl}^T & -I & D_{Cl}^T \\ C_{cl}X_\infty & D_{cl} & -\gamma_i^2 I \end{bmatrix} < 0 \\ X_\infty > 0 \end{cases} \text{for each area}$$
$$ITAE = \int_0^{t_{sim}} (|\Delta f_i| + |\Delta P_{tie-i-k}|)tdk < P_D$$
$$L_j \leqslant x_j \leqslant U_j,\ j = 1, 2, ...,Nv \tag{10}$$

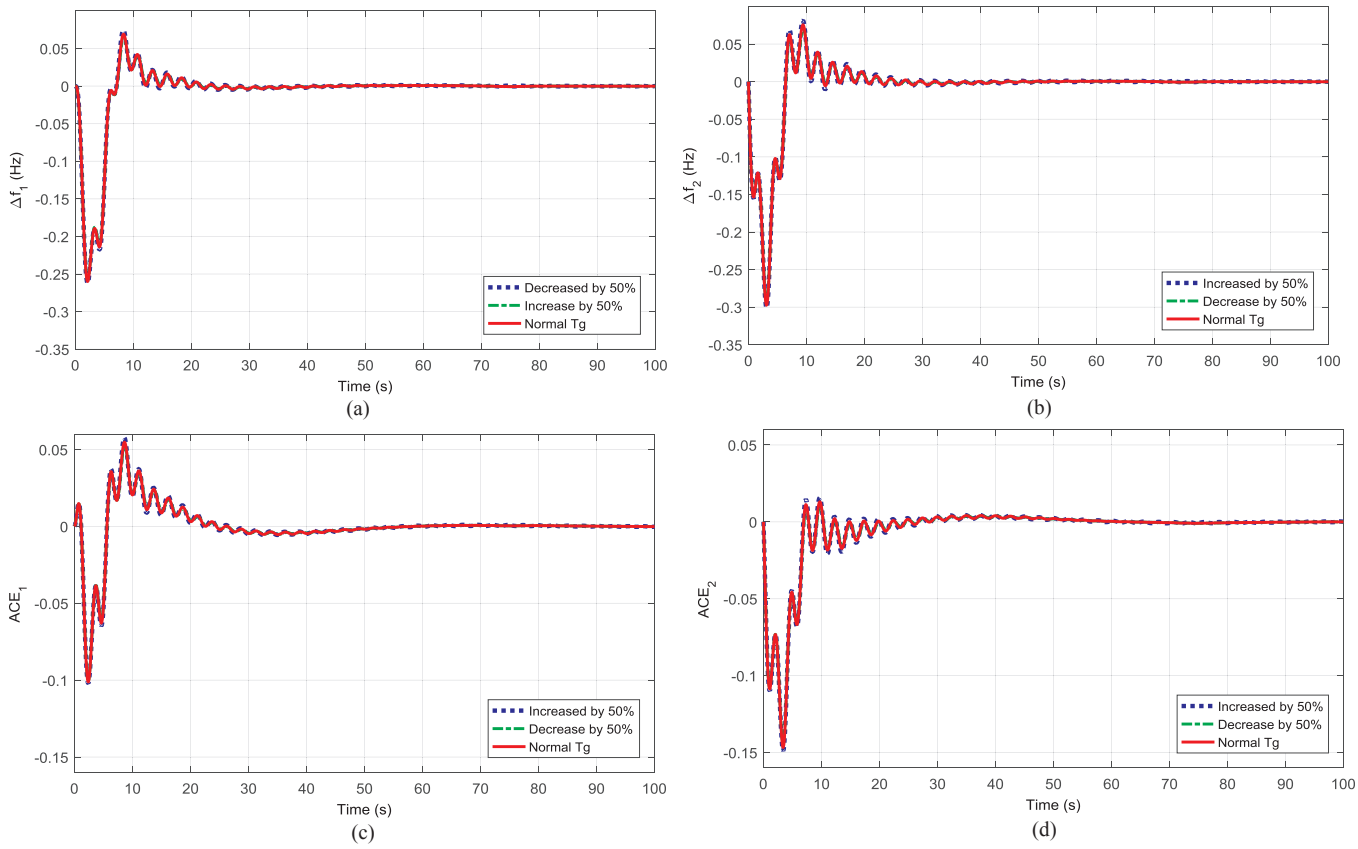

Fig. 9. Comparison of system response subject to Scenario 3 under Experiment I: (a) Δf_1, (b) Δf_2, (c) ACE_1 deviation, (d) ACE_2 deviation.

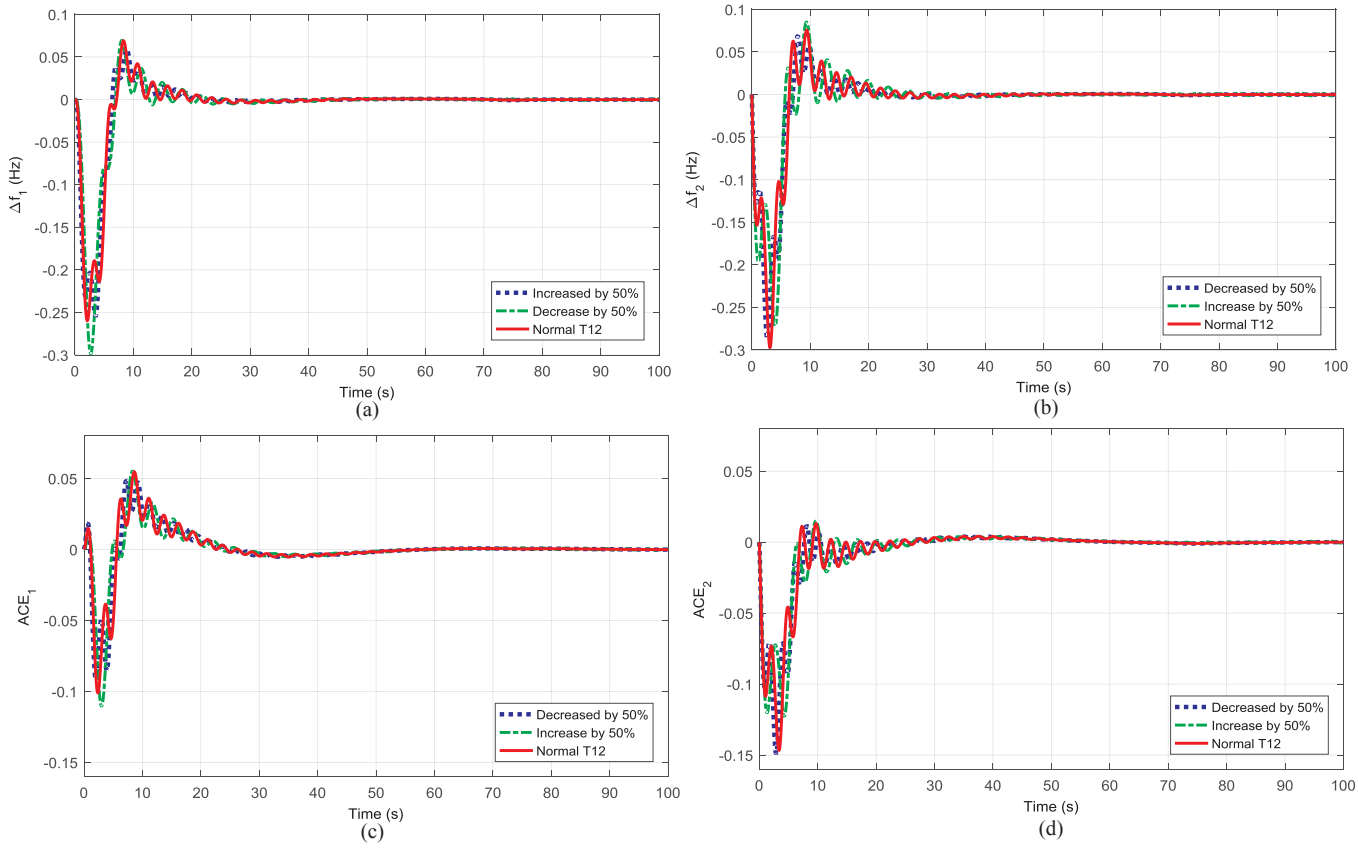

Fig. 10. Comparison of system response subject to Scenario 4 under Experiment I: (a) Δf_1, (b) Δf_2, (c) ACE_1 deviation, (d) ACE_2 deviation.

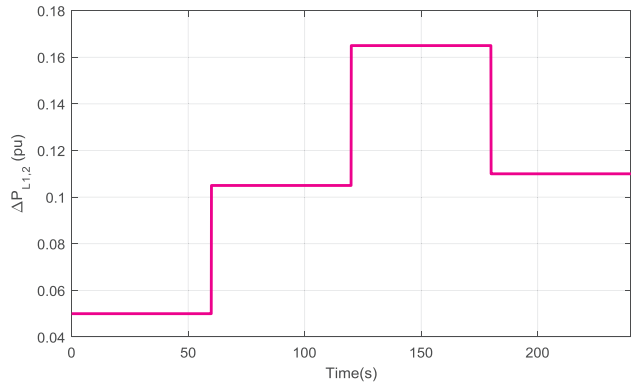

Fig. 11. Dynamical fluctuations of ΔP_{L1}, ΔP_{L2} on Experiment I.

$$\text{Constraint violation } g(X) = \sum_{i=1}^{N} \max(\varepsilon_i, 0) + \max(ITAE - P_D, 0) \tag{11}$$

where γ_i is the robust performance index of area *i*. $g(X)$ is the constraint violation. Δf_i is the frequency deviation in area *i*. $\Delta P_{tie\text{-}i\text{-}k}$ is tie line power deviation between area *i* and area *k*. t_{sim} is simulation time. P_D is the required *ITAE* performance. U_i and L_i are the upper and lower bounds of PI controller parameters, respectively. *Nv* and *N* are the number of PI controller parameters and the number of areas, respectively.

Remark 3. In this study, the FEASP function in MATLAB LMI control toolbox [47] is used to solve the matrix inequality. Note that ε_i is obtained by FEASP function. If ε_i is a positive value, it means the matrix inequality does not have feasible solution. Otherwise, the matrix inequality has feasible solution.

Table 7
Performance comparison of CPSO-LMI-PI and CPEO-LMI-PI for Scenario 5 on Experiment I.

Algorithm	*IAE*	*ITAE*	*ISE*	*ITSE*
CPSO-LMI-PI	79.9434	9331.2488	31.6749	3747.5363
CPEO-LMI-PI	31.3097	3203.2786	10.6382	1104.3712

Remark 4. P_D is the required ITAE performance. Here, we use dynamical P_D during the evolutionary process. Firstly, P_D is set as a very large positive value. Then, when we get feasible solutions the value of P_D is updated by the$\eta \cdot \min(ITAE)$, where min(ITAE) means the minimum value of ITAE in the obtained feasible solutions and η is the positive value. If we set η as a very large value, the required ITAE performance is invalid. If we set η as a very smaller value, it will be difficult for algorithm to find the new feasible solutions. Thus, in this paper, we set η = 1.1.

3.2. Main mechanism of the proposed control scheme

The traditional PEO is proposed for unconstrained optimization problems and it can be improved to handle constrained optimization problems. For optimization, the binary tournament selection is used as constraint-handling method (abbreviated as TCH method) described as follows [46]:

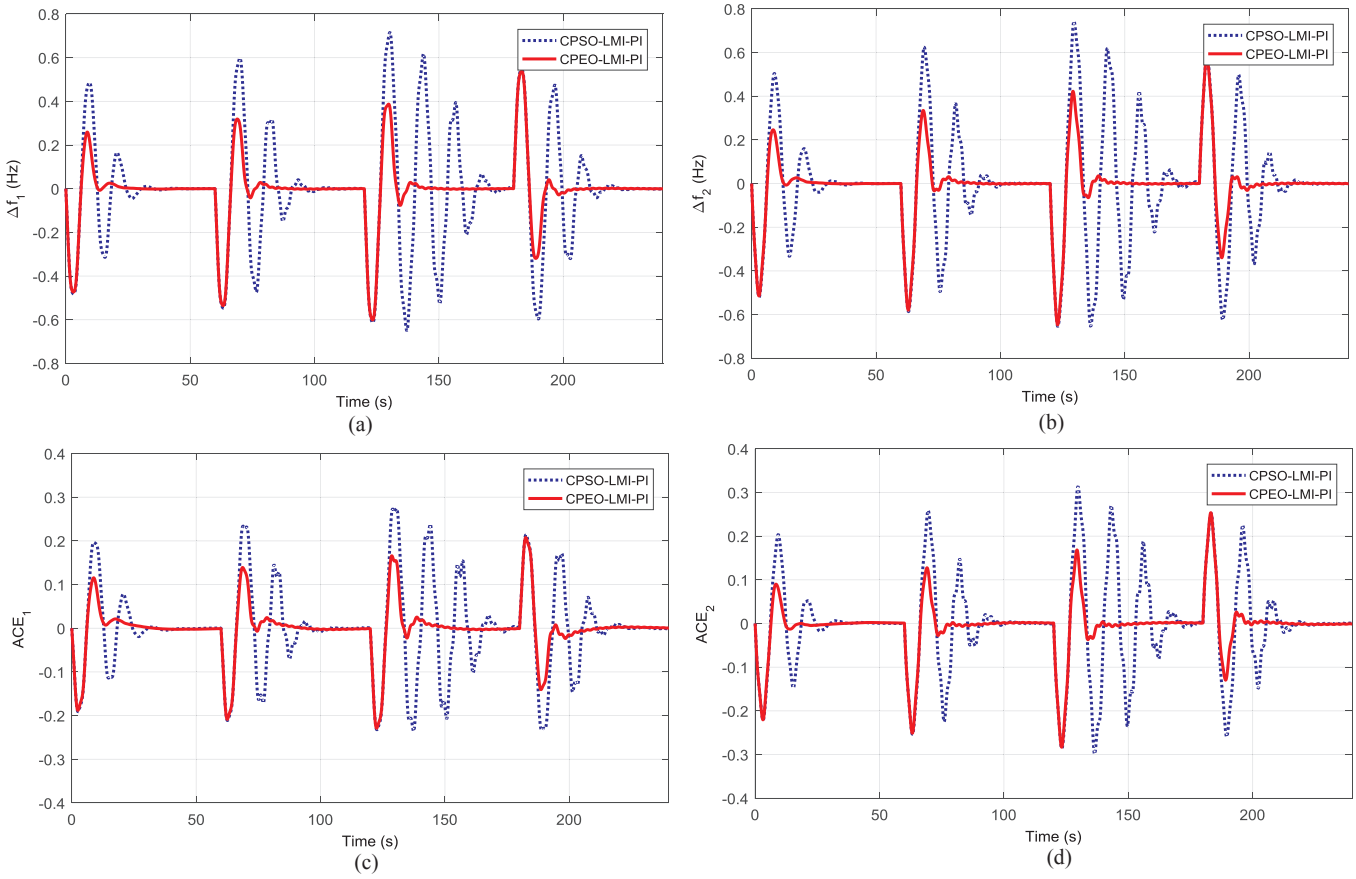

Fig. 12. Comparison of system response subject to Scenario 5 under Experiment I: (a) Δf_1, (b) Δf_2, (c) ACE_1 deviation, (d) ACE_2 deviation.

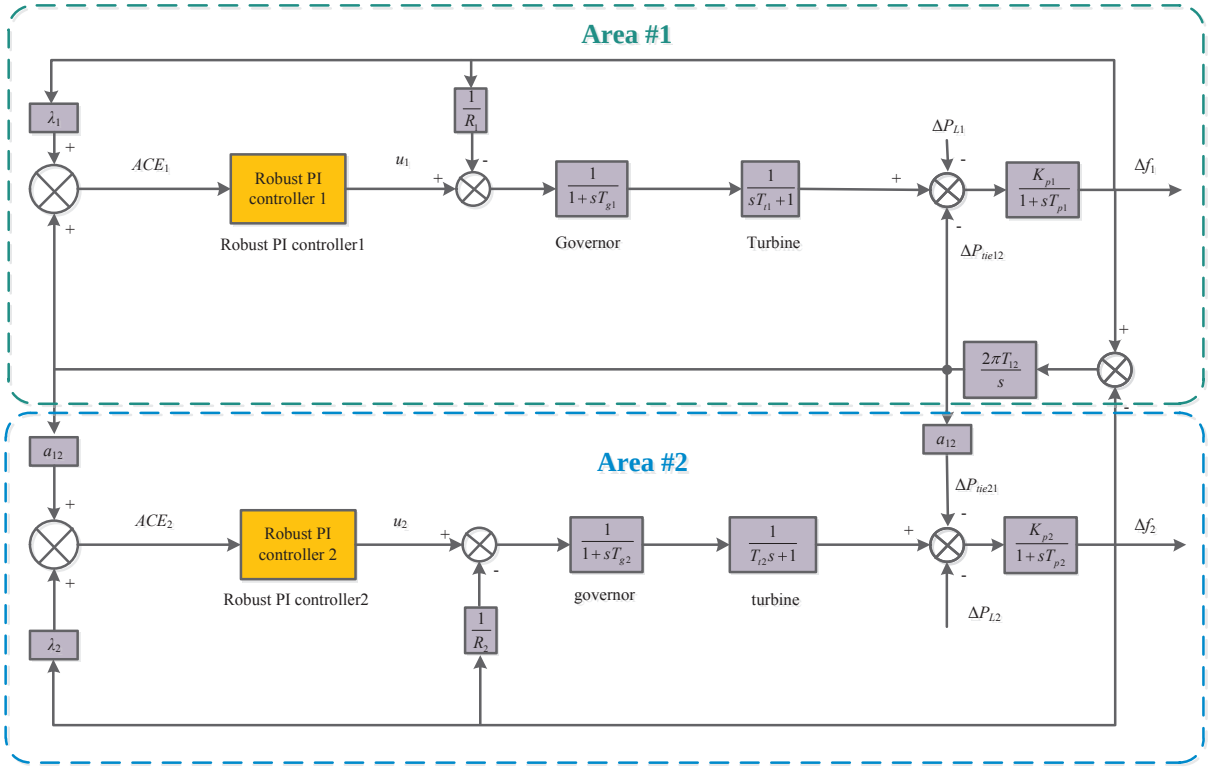

Fig. 13. Two-area interconnected power system under Experiment II [17]

Table 8
The conditions of test scenarios on Experiment II.

Scenarios	Condition
Scenario1	The first area undergoes 0.1 step increase in demand i.e., $\Delta P_{L1} = 0.1$ p.u.
Scenario 2	The second area undergoes 0.1 step increase in demand i.e., $\Delta P_{L2} = 0.1$ p.u.
Scenario 3	The first area and second area simultaneously undergo 0.1 step increase in demand i.e., $\Delta P_{L1} = 0.1$ p.u. $\Delta P_{L2} = 0.1$ p.u.
Scenario 4	Parameter variation: Parameter T_g increase and decrease 50%; Parameter T_{12} increase and decrease 50%, 92% under $\Delta P_{L2} = 0.05$ p.u.
Scenario 5	The first area undergoes 0.1 step increase in demand; the second area undergoes dynamical fluctuations of ΔP_{L2}.

Case (1) Both solutions are feasible, the solution with smaller value of $J(X)$ is better.
Case (2) One is feasible whereas the other is infeasible, the feasible solution is better.
Case (3) Both solutions are infeasible, the solution with smaller constraint violation i.e., $g(X)$ is better.

From this, the solution with smaller $g(X)$ or the feasible solution can be able to survive during the process of optimization. Additionally, the meaning of the TCH rule is illustrated in Fig. 4.

The detailed description of CPEO-LMI-PI controller is given as follows.

Input: The power system model with robust PI controller and related parameters including the dimension Nv of decision variable (i.e., K_{PP1}, K_{II1}, …, K_{PPN}, K_{IIN}), the upper and lower of PI tuning parameters, the required *ITAE* performance P_D, the population size NP, and the maximum number of iteration I_{max}.
Output: The best solution S_{best} (i.e., the decision variable K_{PP1}, K_{II1}, …, K_{PPN}, K_{IIN}) and the corresponding fitness value C_{best}.
Step 1: The N robust PI controllers are encoded into a configuration in CPEO. More specifically, an initial population $\mathbf{P_I} = \{S_1, S_2, \ldots, S_{NP}\}$ is initialized with NP randomly generated solution vectors, where each solution vector $S_l = [K_{PP1}, K_{II1}, \ldots, K_{PPN}, K_{IIN}]$ represents N robust PI controllers in multi-area power system. For better understanding, the detailed generating process of S_l is shown in formulas (12) and (13). In addition, in order to guarantee the initial solution is feasible. Here, the following condition is used. If these exists at least one feasible, then set $\mathbf{P} = \mathbf{P_I}$, $S_{best} = \mathrm{PI}_{be}$ (PI_{be} is the best solutions in $\mathbf{P_I}$), and $C_{best} = C(S_{best})$(the fitness value of S is termed as $C(S)$). Otherwise, go to **Step 1** to re-generate the initial population.

$$S_l = L + (U-L)\cdot R(0,1),\ \ l = 1,\ 2,\ \ldots, NP \tag{12}$$

$$S_l(x_j) = L_j + (U_j-L_j)\cdot R_j(0,1),\ \ j = 1,\ 2,\ \ldots, Nv \tag{13}$$

where $R(0,1)$ is set of uniformly distribution random values between 0 and 1, $S_l(x_j)$ means the value of the variable x_j in S_l, and $R_j(0,1)$ means the j-th element of $R(0,1)$, L and U are the lower and upper bounds of PI controllers.
Step 2: For each solution vector S_l in $\mathbf{P}$:
(a) Obtain the Nv candidate configurations $\{S_{lk},\ (k = 1, 2, 3, \ldots,$

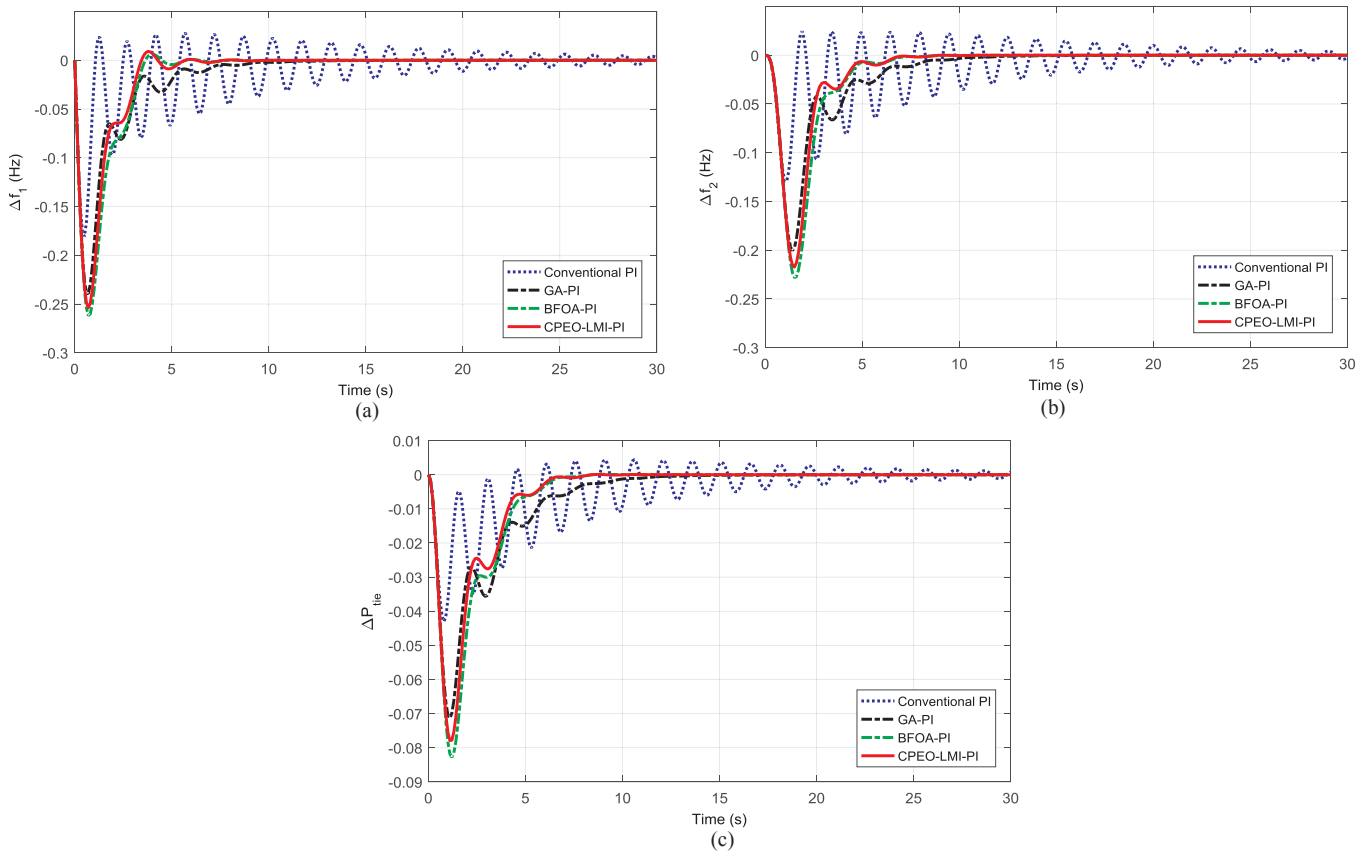

Fig. 14. Comparison of system response subject to Scenario 1 under Experiment II: (a) Δf_1, (b) Δf_2, (c) ΔP_{tie}.

Table 9
Performance comparison of BFOA-PI and CPEO-LMI-PI for Scenario 1 on Experiment II.

Algorithm	*IAE*	*ITAE*	*ISE*	*ITSE*
BFOA-PI	1.0290	1.8372	0.1407	0.1865
CPEO-LMI-PI	0.9199	1.6092	0.1185	0.1473

Nv)} by employing multi-non-uniform mutation (MNUM) operation [49], which is shown in formulas (14)–(15), on the *i*-th component with the others unchanged, then fitness value for each configuration is calculated using formulas (9)–(11).

$$S_l(x_j) = \begin{cases} S_l(x_j) + (U_j - S_l(x_j)) \times A(t), & if \quad r < 0.5 \\ S_l(x_j) + (S_l(x_j) - L_j) \times A(t), & if \quad r \geqslant 0.5 \end{cases} \tag{14}$$

$$A(t) = \left[r_1 \left(1 - \frac{t}{I_{\max}} \right) \right]^b \tag{15}$$

where xj is the decision variable, Uj and Lj are the upper and lower of j-th dimension of decision variable, t is the current number of iteration, r and r1 are uniformly distributed random numbers between 0 and 1, and b is the parameter used in MNUM operation.

(b) Access each configuration according to the fitness function C(Slk). Then, rank the Nv configurations {Slk, (k = 1, 2, 3, …, Nv)} based on the TCH method.

(c) Select the best configuration in {Slk, (k = 1, 2, 3, …, Nv)} based on the rank index, and denote it as Sbl and the corresponding best fitness value as Cbl. Then store Sbl and Cbl in Pb and Cb, respectively.

Step 3: Update the best solution and the corresponding fitness. In other word, if C_{nb} (the best fitness in $\mathbf{C_b}$) is better than C_{best}, then set $C_{best} = C_{nb}$ and $S_{best} = S_{nb}$ (the best solution in $\mathbf{P_b}$).

Step 4: Unconditionally, accept $\mathbf{P} = \mathbf{P_b}$.

Step 5: Obtain the optimal settings of PI controllers and corresponding fitness value C_{best} when the termination criterion is met, otherwise go to step 2 with the **P**.

The flowchart of the proposed CPEO-LMI-PI control scheme is shown in Fig. 5.

3.3. Analysis of the proposed control scheme

As discussed in [37], GA are population-based evolutionary algorithms equipped with selection, crossover and mutation operation for each individual, and PSO are also metaheuristics search techniques based on updating position and velocity for each particle in the group, respectively. By contrast, as mentioned in Section 3.2, the search process of CPEO is mainly determined by mutation operation, which indicates the CPEO search technique with advantages in coding implements and memory requirements. Additionally, the proposed CPEO-LMI-PI is easier than other published evolutionary algorithms (e.g. GA [49], PSO [28], IEA [50]), from the perspective of adjustable parameters, because the number of the adjustable parameters used in constrained PEO is less than that of these published evolutionary algorithms. Moreover, the CPEO is inspired by self-organized criticality (SOC) instead of using the direct gradient information to solve various problems such as non-smooth, multi modal and non-continuous problems, which indicates the CPEO is better to solve the practical engineering problem. Furthermore, as reported in [21,37], some of

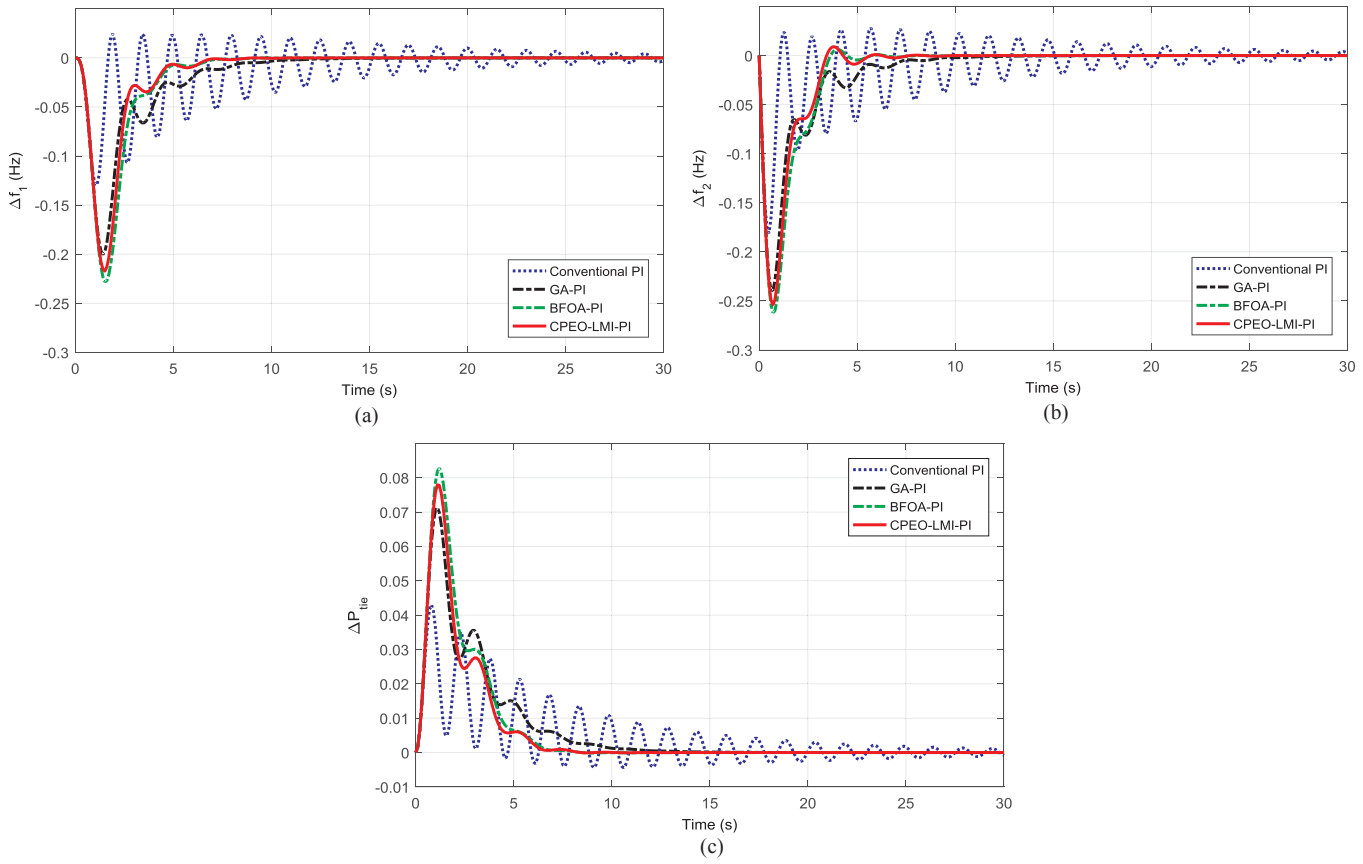

Fig. 15. Comparison of system response subject to Scenario 2 under Experiment II: (a) Δf_1, (b) Δf_2, (c) ΔP_{tie}.

Table 10
Performance comparison of BFOA-PI and CPEO-LMI-PI for Scenario 2 under Experiment II.

Algorithm	*IAE*	*ITAE*	*ISE*	*ITSE*
BFOA-PI	1.0290	1.8372	0.1407	0.1865
CPEO-LMI-PI	0.9199	1.6092	0.1185	0.1473

Table 11
Performance comparison of BFOA-PI and CPEO-LMI-PI for Scenario 3 under Experiment II.

Algorithm	*IAE*	*ITAE*	*ISE*	*ITSE*
BFOA-PI	1.6837	2.8499	0.4590	0.6215
CPEO-LMI-PI	1.4986	2.4704	0.3782	0.4774

evolutionary algorithms including GA, PSO, ant colony optimization (ACO), and artificial bee colony (ABC) pain from slow convergence in refined search stage and may get struck into local minimum solutions, while PEO has advantages in faster convergence and potential ability in global search. These observations motivate the CPEO approach to tune the robust PI controller. Regarding the stability of the CPEO-LMI-PI, the proposed controller is a PI-type controller for LFC problem. The reference [51] presented the stability of PI controller under constant and time-varying delays. The interested readers can refer to [51] for more detail.

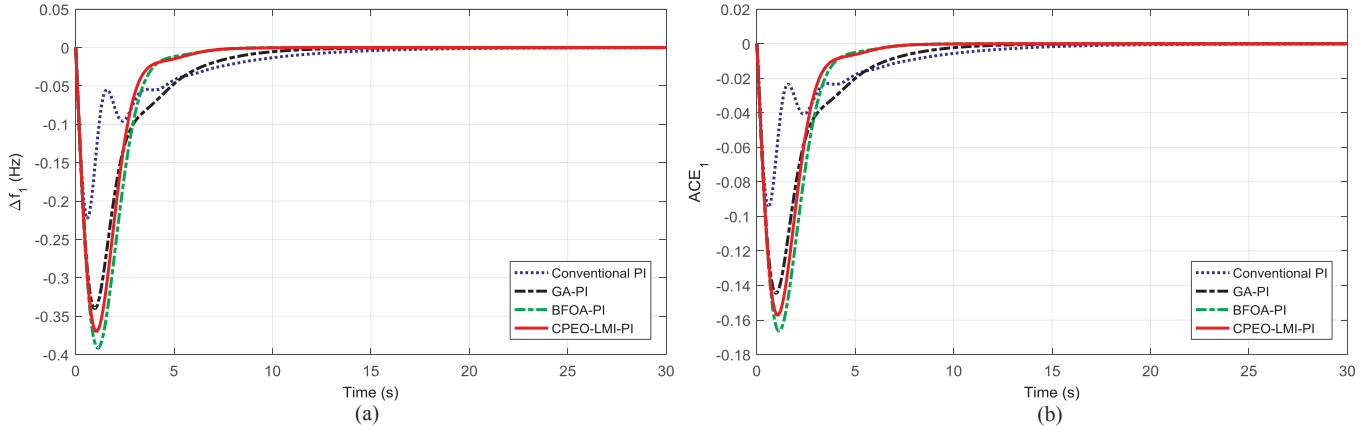

Fig. 16. Comparison of system response subject to Scenario 3 under Experiment II: (a) Δf_1, (b) ACE_1 deviation.

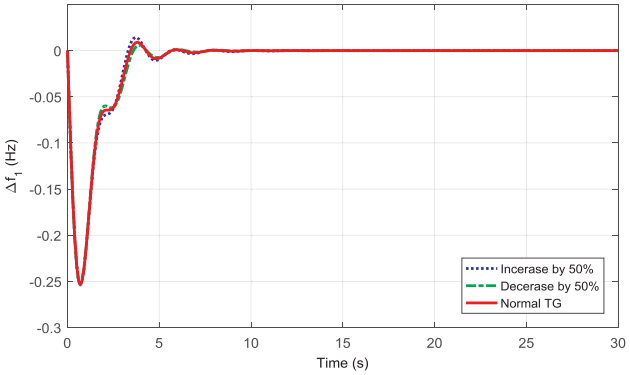

Fig. 17. Frequency deviation Δf_1 obtained by CPEO-LMI-PI under T_g increasing 50%, decreasing 50, and normal condition.

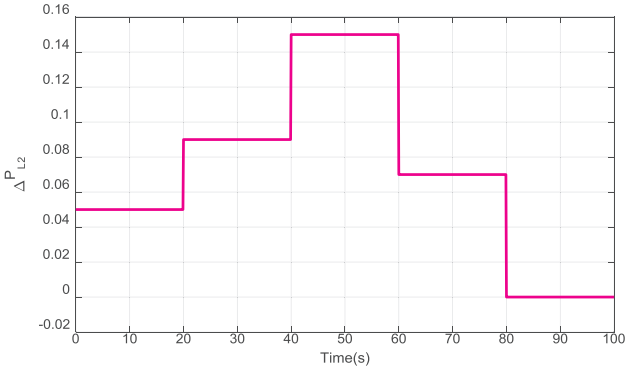

Fig. 19. Dynamical fluctuations of ΔP_{L2}.

4. Simulation results

In order to investigate the performance of the proposed CPEO-LMI-PI controller, in this section, four different experiments are used by comparing with other controllers. The first one is to compare CPEO-LMI-PI control method with CPSO-LMI-PI controller on a two-area interconnected power system with GDB and GRC nonlinearities. The purpose is to demonstrate that the superiority of the proposed CPEO algorithm as the optimizer to search the optimal PI parameters is better than CPSO algorithm. In the second part, we use the same power system as the previous reported work in [17] and the published BFOA-PI [17], GA-PI [17], and conventional PI controller [17] are chose as competitors. The purpose of this part is to validate the superiority of the proposed PI controller to other existing methods. In the third part, we use a two-area interconnected hydro-thermal power system with GDB, GRC, boiler dynamics, and constant time delays to verify the performance of CPEO-LMI-PI by comparing GA-PI [30] conventional PI controller [30], and BIA-MPC [30]. In addition, we extend the proposed controller to a large scale system i.e., a three-area interconnected power system as the fourth experiment. The aim is to show our work can extend to a large scale system. In order to make the readers understand the different between these four experiments, the main differences are shown in Table 1. It should be noted that all the computer simulations in this paper are conducted on a 2.5 GHz and 8 GB RAM computer in the MATLAB2014a software.

4.1. Experiment I

In Experiment I (the model shown in Fig. 2), we compare CPEO-LMI-PI with CPSO-LMI-PI to show the effectiveness of CPEO. In order to purely verify the effectiveness of CPEO algorithm, CPSO uses the same initial population (i.e., swarm) as the one used in CPEO. And same ranges of PI controller are used. Here, as recommend in [17], typical ranges of the optimized parameters are considered as $[-2$ to $10]$. Considering the impact of randomness caused by evolutionary algorithms, the experiment is run 10 times and then the best one is selected. Table 2 shows the parameters of CPSO-LMI-PI and CPEO-LMI-PI used in the experiments and corresponding best controllers, while Table 3 presents the objective function values (J) and the convergent generations. Fig. 6 compares the convergence characteristics of the best objective function value. From Fig. 6, it can be seen that the objective function decreases over generations of CPEO and CPSO, and CPEO converges at a faster rate (49 generations) than that of CPSO (62 generations). Additionally, CPEO can search smaller objective fitness than CPSO, so CPEO algorithm can be considered to provide better convergence characteristic than CPSO for optimal design of robust PI controller for interconnected power system. Moreover, it is clear that from the perspective of algorithm design, the proposed CPEO algorithm is simpler than CPSO algorithm, due to its fewer adjustable parameters and only mutation operation. Here, we use five test scenarios of Experiment I to investigate the interconnected power system frequency response. For better readability, Table 4 presents these five scenarios.

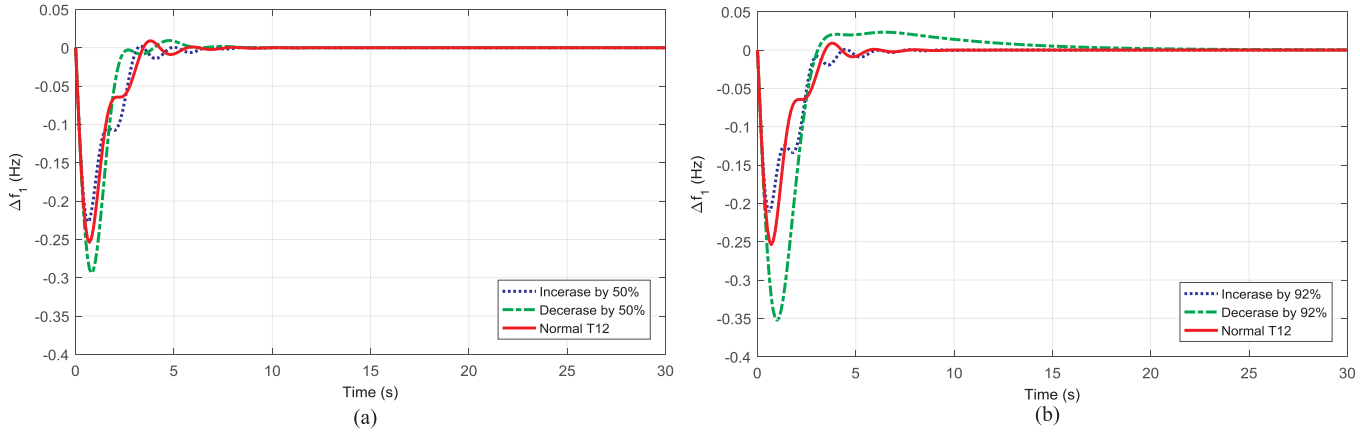

Fig. 18. Frequency deviation Δf_1 obtained by CPEO-LMI-PI (a) under T_{12} increasing 50%, decreasing 50, and normal condition; (b) under T_{12} increasing 92%, decreasing 92%, and normal condition.

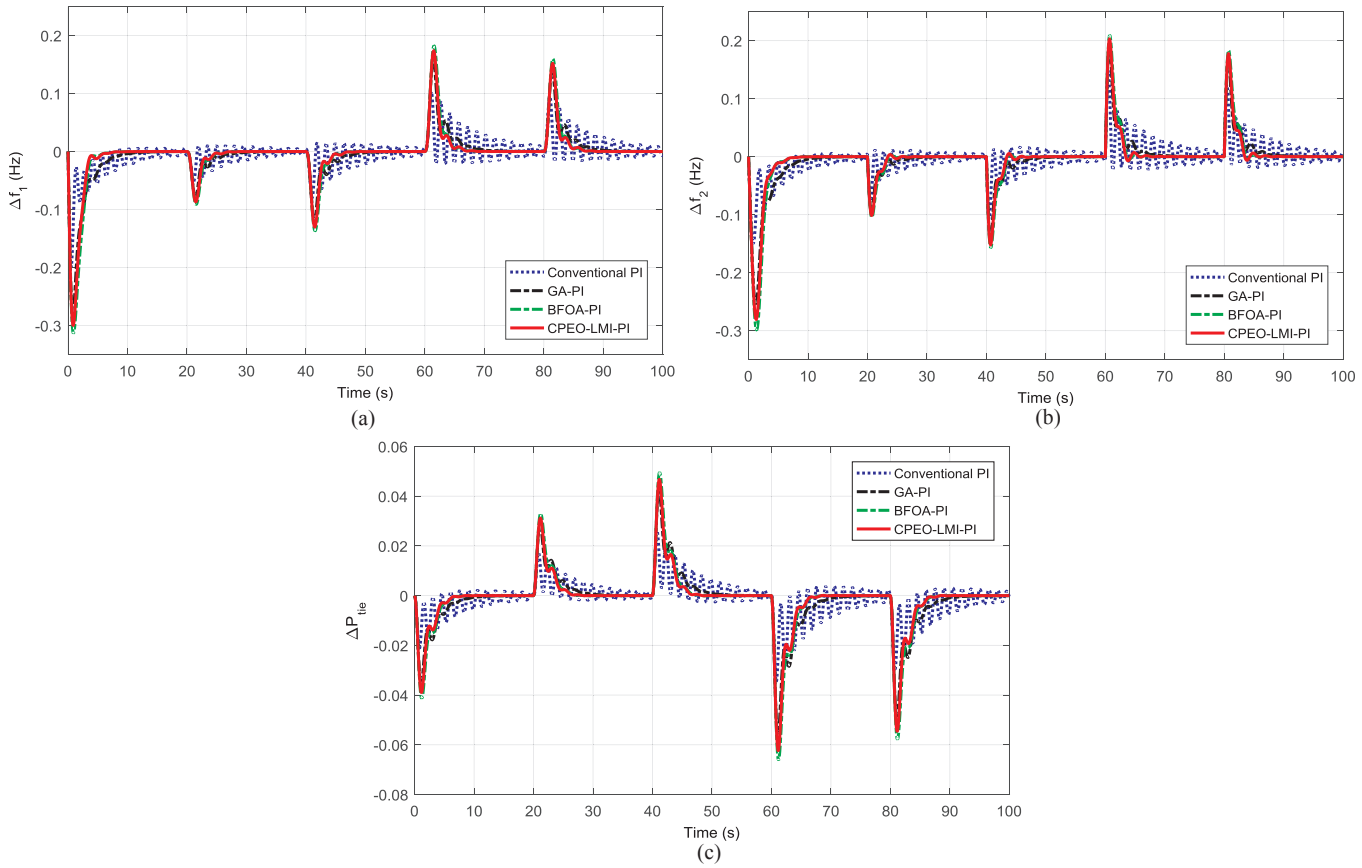

Fig. 20. Comparison of system response subject to Scenario 5 under Experiment II: (a) Δf_1, (b) Δf_2, (c) ΔP_{tie}.

Table 12
Performance comparison of BFOA-PI and CPEO-LMI-PI for Scenario 5 under Experiment II.

Algorithm	*IAE*	*ITAE*	*ISE*	*ITSE*
BFOA-PI	3.925	146.870	0.4967	14.056
CPEO-LMI-PI	3.5035	131.143	0.4142	11.797

Scenario 1: The second area undergoes 0.05 step increase in demand ($\Delta P_{L2} = 0.05$p.u.)

For Scenario 1, the second area undergoes a 0.05 step increase in demand. The Δf and ACE deviation of both areas obtained by CPEO-LMI-PI and CPSO-LMI-PI are shown in Fig. 7(a)–(d). From these figures, the response with CPSO-LMI-PI is suffered from higher settling time and larger oscillations than that of CPEO-LMI-PI. To analysis the quality of the above-mentioned control methods, we use some performance indices such as integral of time multiplied absolute error (*ITAE*), integral of absolute error (*IAE*), and integral of time multiplied squared error (*ITSE*),integral of squared error (*ISE*) defined as follows:

$$ITAE = \int_0^{t_{sim}} (|\Delta f_1| + |\Delta f_2| + |\Delta P_{tie}|)t\,dt, \tag{16}$$

$$IAE = \int_0^{t_{sim}} (|\Delta f_1| + |\Delta f_2| + |\Delta P_{tie}|)dt, \tag{17}$$

$$ITSE = \int_0^{t_{sim}} ((\Delta f_1)^2 + (\Delta f_2)^2 + (\Delta P_{tie})^2)t\,dt. \tag{18}$$

$$ISE = \int_0^{t_{sim}} ((\Delta f_1)^2 + (\Delta f_2)^2 + (\Delta P_{tie})^2)dt, \tag{19}$$

where Δf_1, Δf_2 are the frequency deviations in the first area and the second area respectively. ΔP_{tie} is tie line power deviation and t_{sim} is simulation time. Smaller performance indices indicate a better control performance.

The corresponding control performance is tabulated in Table 5. Similar observation can be found from Table 5, where the proposed CPEO-LMI-PI is better than CPSO-LMI-PI in terms of the performance indices.

Scenario 2: Both area 1 and area 2 undergo 0.05 step increase in demand ($\Delta P_{L1} = 0.05$p.u, $\Delta P_{L2} = 0.05$ p.u.)

When the tested system undergoes Scenario 2, the signals of the closed loop system are shown in Fig. 8 and the corresponding control performance is presented in Table 6. Remarkably, CPSO-LMI-PI controller shows worse performance than CPEO-LMI-PI. More specially, the increased overshooting and settling time are obtained by CPSO-LMI-PI while the proposed CPEO-LMI-PI shows less overshooting and settling time. As a consequence, the CPEO-LMI-PI is prior to CPSO-LMI-PI on Scenario 2.

Scenario 3: Parameter T_g increase and decrease 50% under $\Delta P_{L2} = 0.05$ p.u.

In order to test the robustness of the proposed CPEO-LMI-PI control scheme against parameters uncertainties, the simulation has been made when parameter T_g increases and decreases 50% under $\Delta P_{L2} = 0.05$ p.u. Fig. 9 presents the system response undergoing Scenario 3. It is obvious

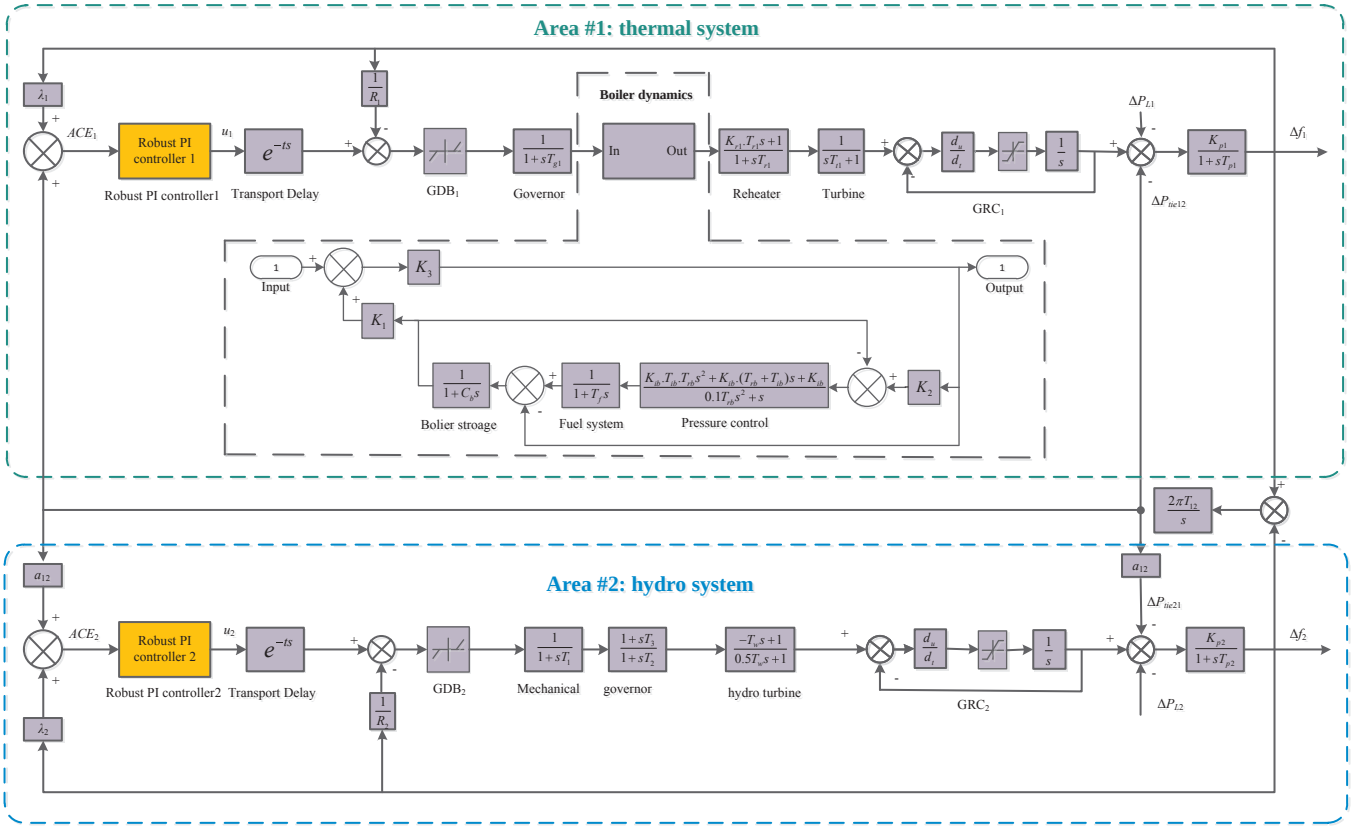

Fig. 21. Two-area nonlinear interconnected power system under Experiment III [30]

Table 13
The conditions of test scenarios under Experiment III.

Scenarios	Condition
Scenario1	The hydro-thermal system undergoes step increase in demand and subjected to 2 s transport time delays, i.e., ΔP_{L1} = 0.015p.u, ΔP_{L2} = 0.015p.u, t = 2 s.
Scenario 2	The hydro-thermal system undergoes step increase in demand and subjected to 15 s transport time delays, i.e., ΔP_{L1} = 0.01p.u, ΔP_{L2} = 0.01p.u, t = 15 s.
Scenario 3	Parameter T_{12} increase and decrease 50% (or 90%) under ΔP_{L1} = 0.015p.u, ΔP_{L2} = 0.015p.u and t = 2 s.
Scenario 4	The two area are simultaneously under dynamical fluctuations of ΔP_{L1}, ΔP_{L2} and t = 2 s.

that the system is stable with the proposed CPEO-LMI-PI controller.

Scenario 4: Parameter T_{12} increase and decrease 50% under ΔP_{L2} = 0.05 p.u.

Another parameter T_{12} variation test is also used to further investigate the robustness of the proposed design. To carry out this test, we assume T_{12} increases and decreases 50% under ΔP_{L2} = 0.05 p.u. Note that the wide range of parameter T_{12} uncertainty will account for poor coupling between the two areas. The corresponding Δf and ACE deviations under this condition are shown in Fig. 10. From Fig. 10, it can be seen that the designed controller can be capable of providing stable results, which confirms the robustness of the proposed controller.

Scenario 5: Both area 1 and area 2 undergo dynamical fluctuations

In this Scenario, the dynamical loads fluctuations of ΔP_{L1} and ΔP_{L2} are considered to demonstrate the effectiveness of the proposed CPEO-LMI-PI control method compared to CPSO-LMI-PI controller. Fig. 11 shows the dynamical loads disturbances of ΔP_{L1} and ΔP_{L2}. Fig. 12(a)–(d) show the frequency response behavior of power system. Obviously, the proposed CPEO-LMI-PI outperforms CPSO-LMI-PI controller because it has faster transient responses and less oscillation of Δf_1, Δf_2, ACE_1 and ACE_2, which also indicates that the CPEO-LMI-PI controller's efficiency is better than that of CPSO-LMI-PI. Moreover, Table 7 presents the performance indices (i.e., *ITAE*, *IAE*, *ITSE*, *ISE*) obtained by CPSO-LMI-PI and CPEO-LMI-PI. The results in Table 7 indicate that the proposed CPEO-LMI-PI method consistently outperforms the CPSO-LMI-PI control method in term of these indices.

4.2. Experiment II

In Experiment II, we use another two-area interconnected power system reported in previous work [17] to demonstrate the efficiency of the proposed control approach by comparing the published PI-based LFC methods i.e., BFOA-PI [17], GA-PI [17] and conventional PI [17]. The schematic diagram of system is shown in Fig. 13, and corresponding parameters are given in Appendix A.2. For a fair comparison, the parameters of this power system are set as the same as in [17] and

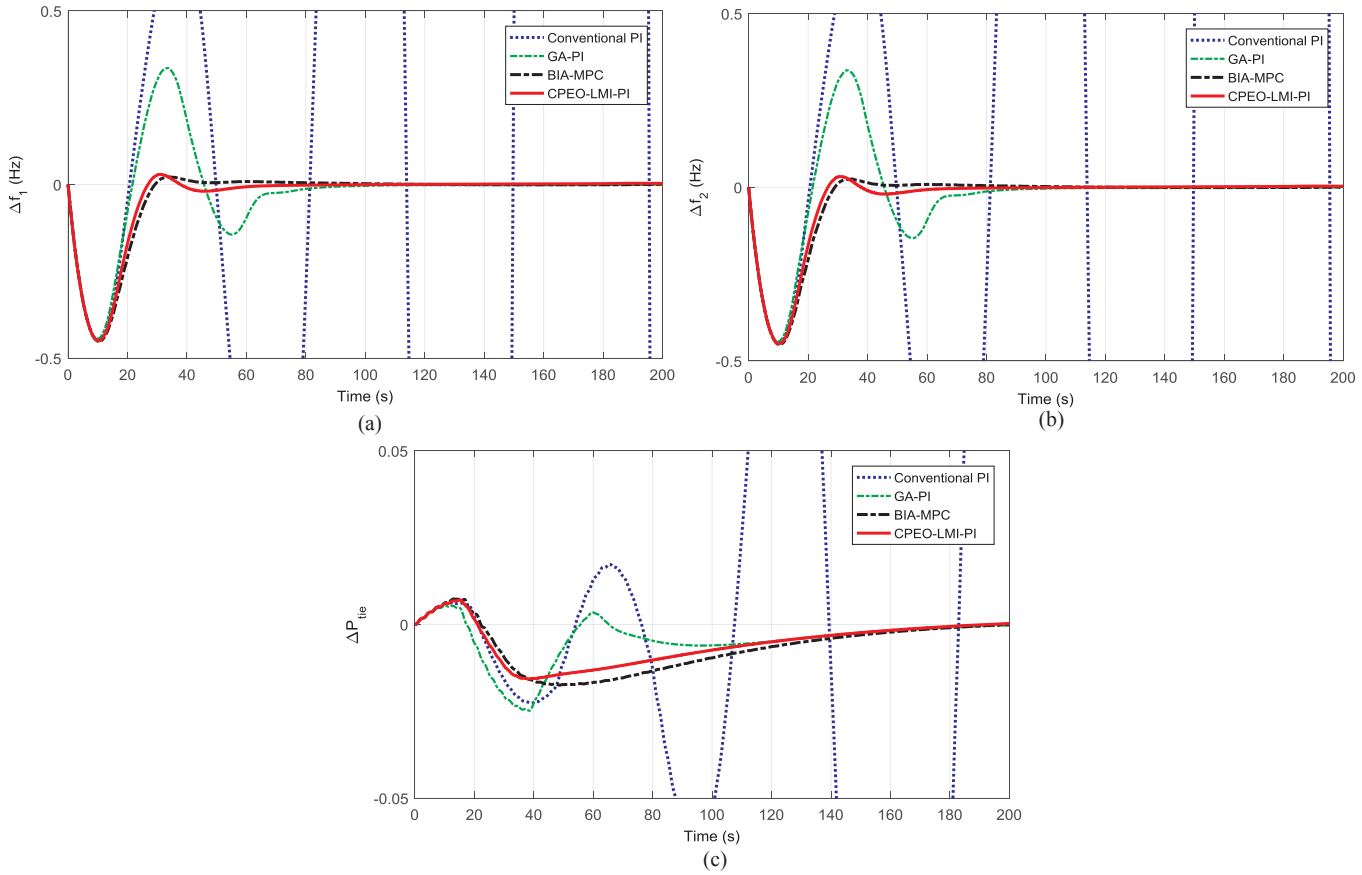

Fig. 22. Comparison of system response subject to Scenario 1 under Experiment III: (a) Δf_1, (b) Δf_2, (c) ΔP_{tie}.

the parameters of three PI controllers are directly taken from [17]. The optimal values of robust PI controller optimized by CPEO-LMI-PI are $0.3631(K_{PP1} = K_{PP2} = 0.3631)$ and $-0.3104(K_{II1} = K_{II2} = -0.3104)$ for this experiment. Here, five scenarios are considered in Experiment II listed in Table 8. Note the first third scenarios are the same as in [17]. The fourth Scenario is to confirm the robustness of the proposed design again system parameters uncertainties. And the fifth Scenario is used to demonstrate CPEO-LMI-PI controller is superior to BFOA-PI, GA-PI and conventional PI for the dynamical loads fluctuations of ΔP_{L2}.

Scenario 1: The first area undergoes 0.1 step increase in demand ($\Delta P_{L1} = 0.1$p.u.)

For Scenario 1 under Experiment II, a 0.1 step increase in demand of the first area is used. The Δf in both areas and ΔP_{tie} obtained by conventional PI, GA-PI, BFOA-PI and CPEO-LMI-PI are shown in Fig. 14. From Fig. 14, the BFOA-PI and CPEO-LMI-PI obviously outperform GA-PI and conventional PI. Here, we list the control performance indices (i.e., *IAE*, *ITAE*, *ISE*, *ITSE*) to further compare CPEO-LMI-PI with BFOA-PI and the results are shown in Table 9. Clearly, from Table 9, it can be seen that the proposed CPEO-LMI-PI is slightly better than BFOA-PI in terms of the performance indices. Overall, the CPEO-LMI-PI can achieve better ensemble control performance than BFOA-PI, GA-PI and conventional PI under this scenario.

Scenario 2: The second area undergoes 0.1 step increase in demand ($\Delta P_{L2} = 0.1$p.u.)

A 0.1 step increase in demand of the second area is used as the second Scenario. The Δf in both areas and ΔP_{tie} obtained by four different PI controllers are shown in Fig. 15. In addition, the Table 10 presents the performance indices of BAFO-PI and CPEO-LMI-PI. From these figures and Table 10, similar observation can be found with scenario 1 that the ensemble control performance of the proposed CPEO-LMI-PI control strategy is the best. Note that the performance indices in Scenario 1 and Scenario 2 are the same because the two areas in this power system model are the same and the same value of step increase in demand is applied.

Scenario 3: Both area 1 and area 2 undergo 0.1 step increase in demand ($\Delta P_{L1} = 0.1$p.u, $\Delta P_{L2} = 0.1$ p.u.)

In this scenario, the first area and second area simultaneously undergo 0.1 step increase in demand i.e., $\Delta P_{L1} = 0.1$ p.u. $\Delta P_{L2} = 0.1$ p.u. Fig. 16(a) and (b) show the frequency response behavior and ACE of the first area, respectively. For Fig. 16, it can be found that the results have the same trends. This is because the area 1 and area 2 have same structure and we use the same step increase in demand. In a word, the ΔP_{tie} is zeros and the value of ACE_1 is λ_1 times larger than Δf_1. Besides, the Table 11 shows the performance indices obtained by BFOA-PI and CPEO-LMI-PI. Critical observation of Fig. 16 and Table 11, it demonstrates that the ensemble control performance of proposed CPEO-LMI-PI controller is better than other control strategies.

Scenario 4: Parameter variation

This scenario is devoted to assessing the robustness of the proposed controller again parameters uncertainties of this power system model.

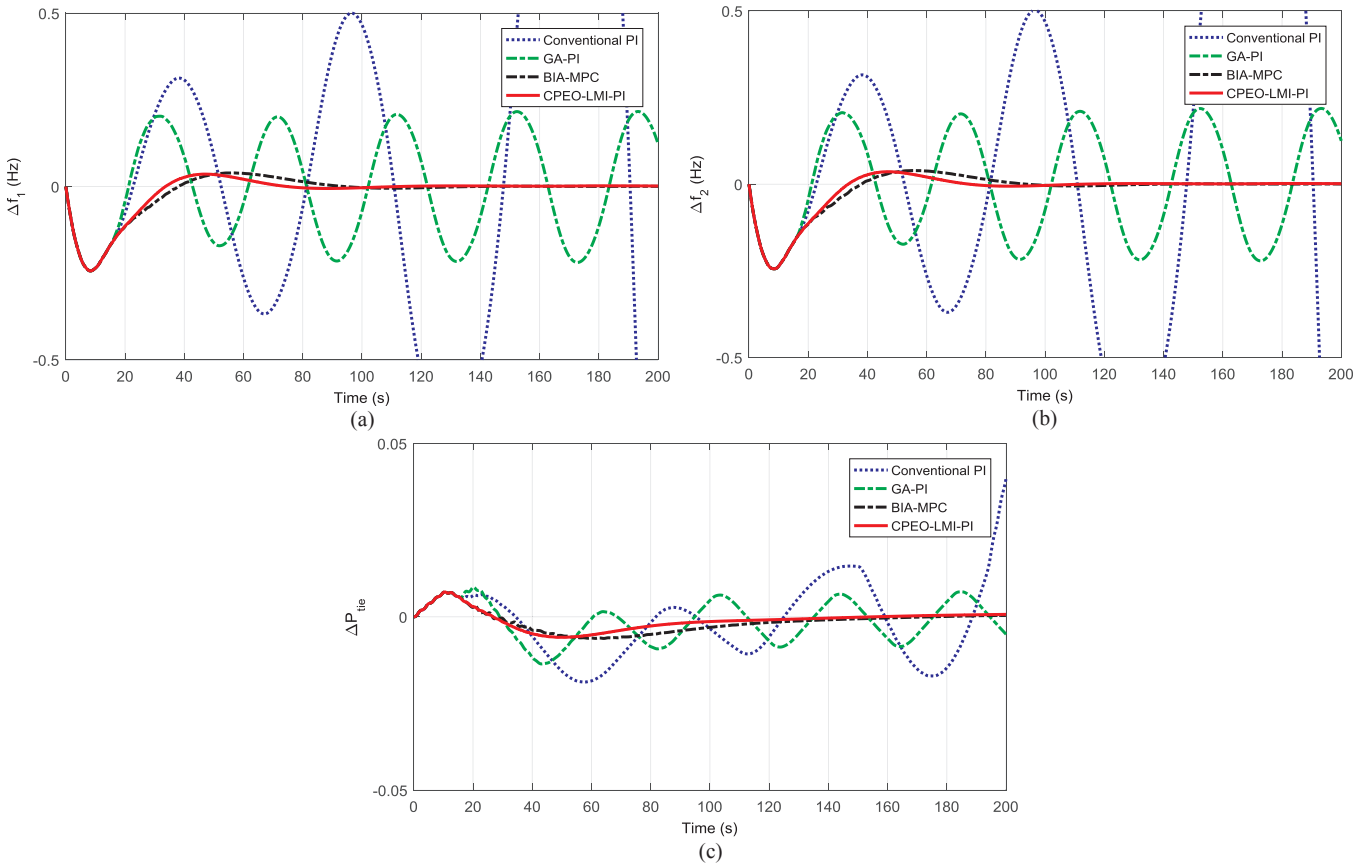

Fig. 23. Comparison of system response subject to Scenario 2 under Experiment III: (a) Δf_1, (b) Δf_2, (c) ΔP_{tie}.

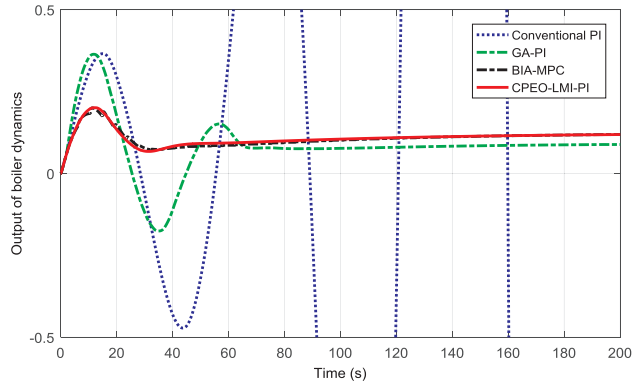

Fig. 24. Comparison of boiler dynamics output obtained by three PI controllers.

Fig. 17 shows the results under two conditions including T_g increasing 50% and decreasing 50% when $\Delta P_{L1} = 0.1$; It is clear that system is stable with the CPEO-LMI-PI controller. Additionally, another parameter T_{12} is used to validate the robustness of the proposed controller because the T_{12} may account for strong coupling between two areas. Here, four conditions are applied including increasing 50%, decreasing 50%, increasing 92% and decreasing 92% when $\Delta P_{L1} = 0.1$. Fig. 18 presents the response of frequency with variation T_{12}. The proposed controller can provide sufficient stable results and the robustness of the proposed controller is demonstrated.

Scenario 5: The area 1 undergoes 0.1 step increase in demand and area 2 undergoes dynamical fluctuations

Fig. 19 shows the dynamical loads disturbances of ΔP_{L2}. Fig. 20(a)–(c) show the frequency response behavior and power deviations, respectively. Table 12 presents the performance comparison (CPEO-LMI-PI and BFOA-PI) when the system undergoes this scenario. It is obvious that *IAE*, *ITAE*, *ISE*, *ITSE* obtained by CPEO-LMI-PI are all better than BFOA-PI. Critical observation of Fig. 20 and Table 12, CPEO-LMI-PI is slightly better than BFOA-PI and is still prior to GA-PI and conventional PI.

4.3. Experiment III

In this Experiment, the performance of the proposed CPEO-LMI-PI is investigated on a nonlinear hydro-thermal power system shown in Fig. 21 with GRC, GDB, boiler dynamics and time delay. The optimal values of control parameters obtained by CPEO-LMI-PI are 0.0067(K_{PP1}), 0.0327(K_{II1}) for area 1 and 0.3067(K_{PP2}), 0.0146(K_{II2}) for area 2. The typical parameters of system, GRC and GDB are set as [30] shown in Appendix A.3. To demonstrate the performance of CPEO-LMI-PI, the GA-PI, conventional PI and BIA-MPC reported in [30] are considered as the competitors. Table 13 presents four test scenarios for investigating this nonlinear hydro-thermal power system frequency response. The first second scenarios are taken from the reference [30], while the third scenario is designed to confirm the robustness of the proposed controller. The fourth one is used to test its effectiveness

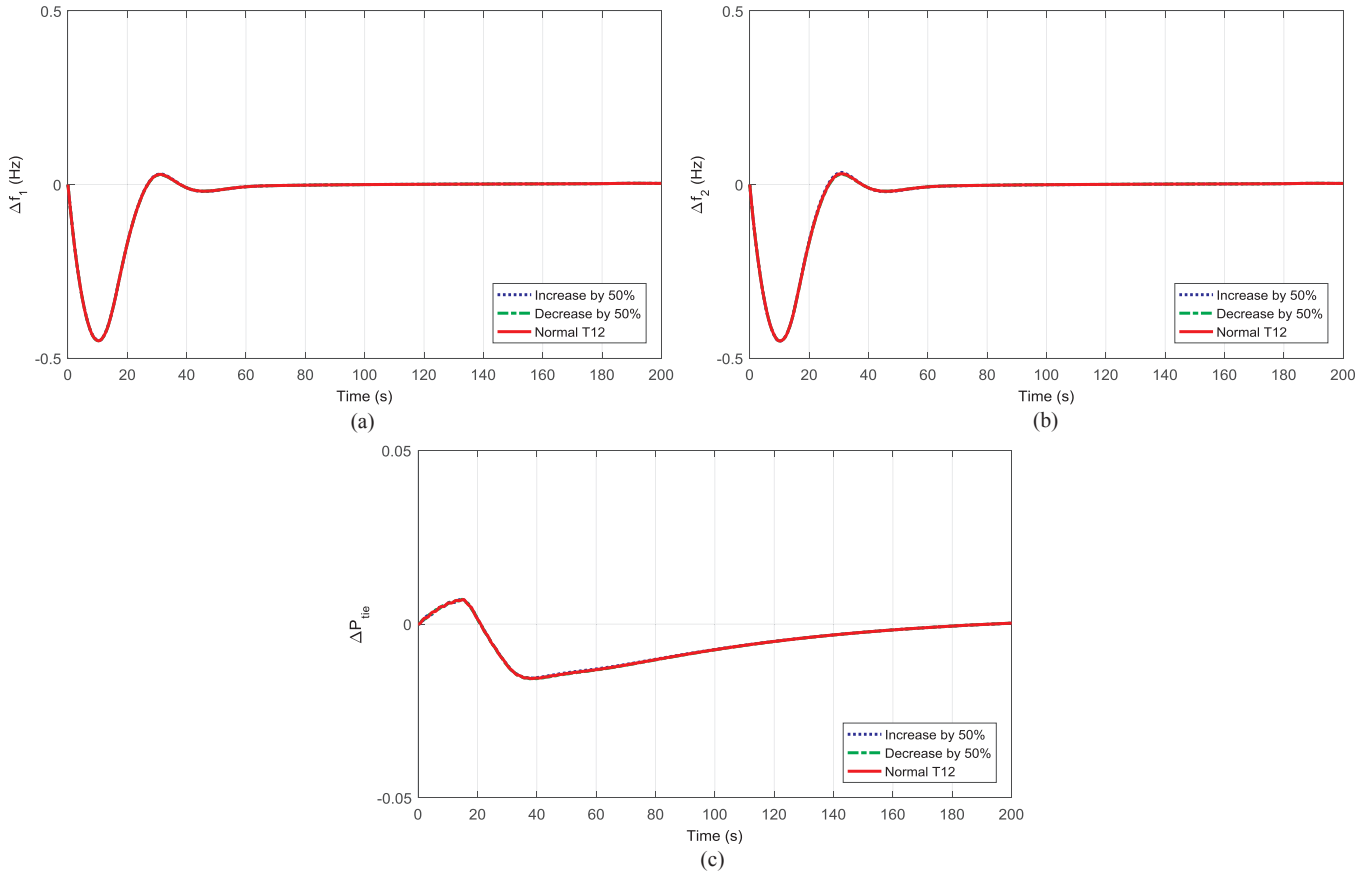

Fig. 25. Comparison of system response subject to Scenario 3 under Experiment III: (a) Δf_1, (b) Δf_2, (c) ΔP_{tie}.

under dynamical fluctuations of ΔP_{L1}, ΔP_{L2}.

Scenario 1: The system undergoes $\Delta P_{L1} = 0.015$p.u, $\Delta P_{L2} = 0.015$p.u step increase and subjects to $t = 2$ s time delays

For Scenario 1, the Δf in both areas and ΔP_{tie} obtained by GA-PI [30], conventional PI [30], BIA-MPC [30] and CPEO-LMI-PI are shown in Fig. 22. From Fig. 22, we can observer that the conventional PI control method is oscillation which is can be acceptable. Also, compared with GA-PI controller, the proposed CPEO-LMI-PI has smaller overshooting and less oscillation, which means that the proposed CPEO-LMI-PI is better than GA-PI and conventional PI in terms of system responses. And, compared with BIA-MPC, we can find these two controllers have similar control performance, but BIA-MPC has more complicated structure than the proposed PI-type controller from an implementation point of view.

Scenario 2: The system undergoes $\Delta P_{L1} = 0.01$p.u, $\Delta P_{L2} = 0.01$p.u step increase and subjects to $t = 15$ s time delays

When the tested system undergoes Scenario 2, the results are shown in Fig. 23. Remarkably, traditional PI controller and GA-PI controller fails to maintain system stability because of increased time delays, while the proposed CPEO-LMI control method still shows less overshooting and settling time. Under this scenario, the CPEO-LMI-PI is slightly better than BIA-MPC method. As a consequence, the CPEO-LMI is prior to traditional PI, GA-PI controller and BIA-MPC on Scenario 2. In addition, the Fig. 24 shows the output of boiler dynamics. Obviously, the result obtained by CPEO-LMI-PI and BIA-MPC are stable while that of other control methods are unstable.

Scenario 3: Increasing 50% and decreasing 50% of T_{12} under $\Delta P_{L1} = 0.015$p.u, $\Delta P_{L2} = 0.015$p.u and $t = 2$ s

In scenario 3, besides increasing 50% and decreasing 50% of T_{12}, the system undergoes $\Delta P_{L1} = 0.015$p.u, $\Delta P_{L2} = 0.015$p.u step increase and subjects to time delays $t = 2$ s. That the wide range of parameter T_{12} uncertainty will account for poor coupling between thermal system with hydro system. Simulating the nonlinear model under this condition, the Δf and ΔP_{tie} of power system are given in Fig. 25(a)–(c), respectively. Noticeably, the performance of CPEO-LMI-PI is robustness. In order to further show the robustness of CPEO-LMI-PI, the compared results of conventional PI, GA-PI, and BIA-MPC under increasing 90% and decreasing 90% of T_{12} are given in Figs. 26 and 27. It can be seen that CPEO-LMI-PI is much better than two kinds of PI controller and a bit better than BIA-MPC.

Scenario 4: The system undergoes dynamical loads fluctuations of ΔP_{L1}, ΔP_{L2} and subjects to $t = 2$ s time delays

In this Scenario, the dynamical loads fluctuations of ΔP_{L1} and ΔP_{L2} are considered to demonstrate the effectiveness of the proposed CPEO-

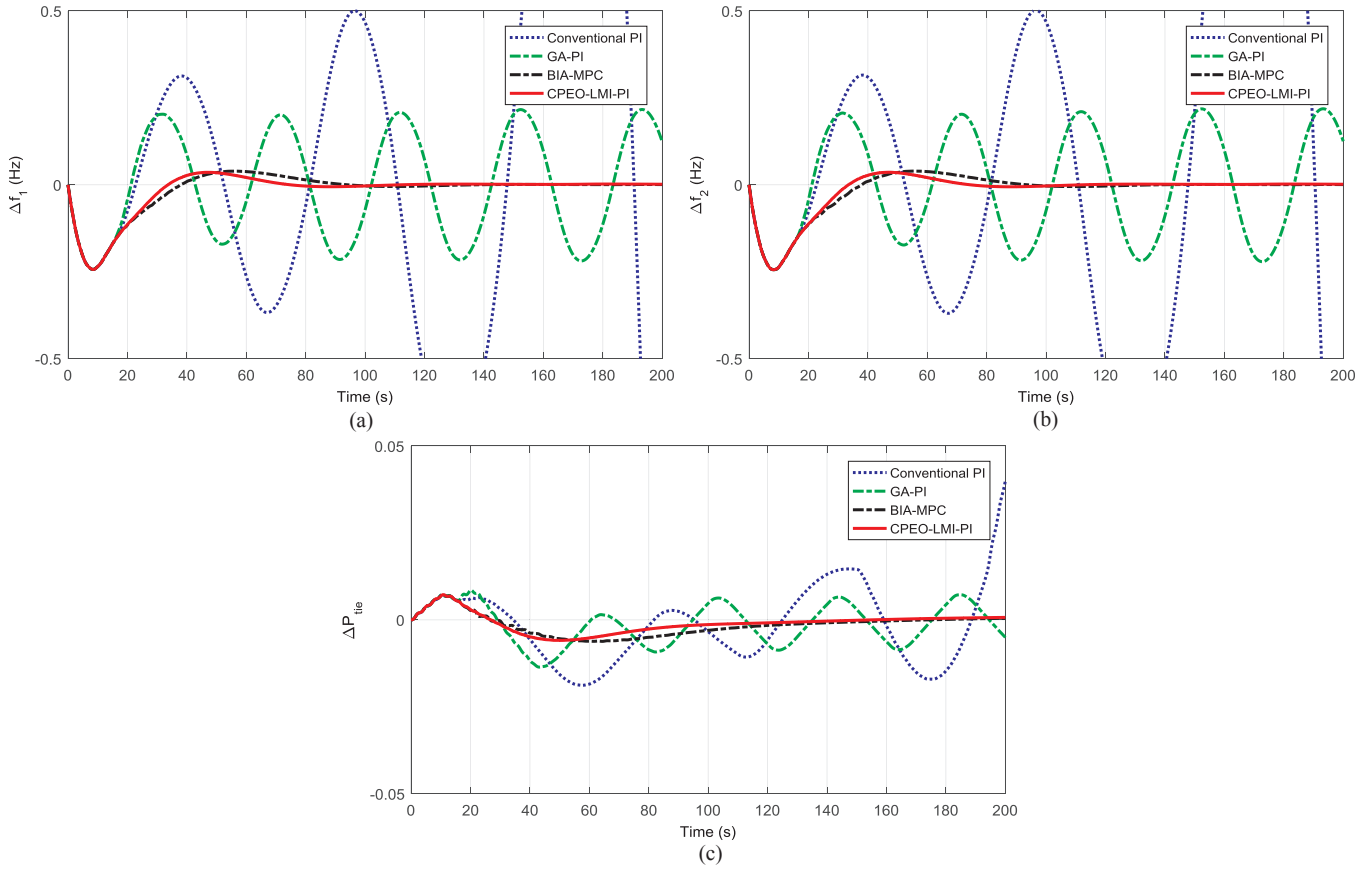

Fig. 26. Comparison of system response subject to Scenario 3 (under T_{12} increasing 90%) on Experiment III: (a) Δf_1, (b) Δf_2, (c) ΔP_{tie}.

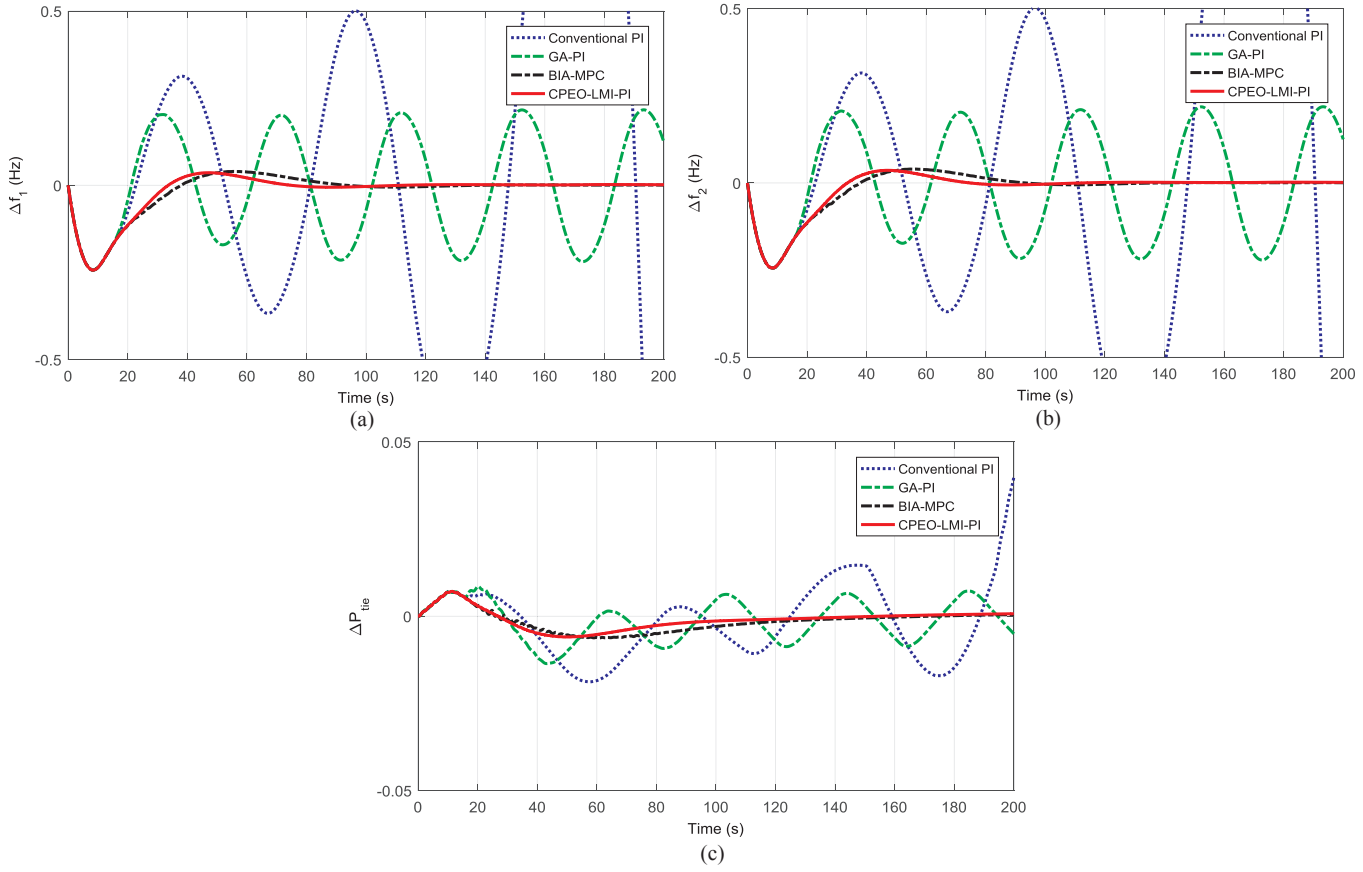

Fig. 27. Comparison of system response subject to Scenario 3 (under T_{12} decreasing 90%) on Experiment III: (a) Δf_1, (b) Δf_2, (c) ΔP_{tie}.

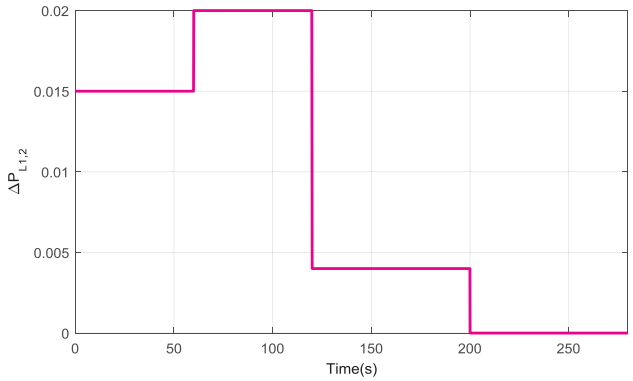

Fig. 28. Dynamical fluctuations of ΔP_{L1}, ΔP_{L2} on Experiment III.

LMI-PI control method compared to GA-PI, conventional PI and BIA-MPC. Fig. 28 shows the dynamical loads disturbances of ΔP_{L1} and ΔP_{L2}. Fig. 29(a)–(c) show the frequency response behavior of nonlinear hydro-thermal system and power deviations ΔP_{tie}, respectively. Obviously, the proposed CPEO-LMI-PI outperforms GA-PI and conventional PI because it has faster transient responses and less oscillation of Δf_1, Δf_2 and ΔP_{tie} and it has similar performance with BIA-MPC.

Overall, the proposed robust PI controller is much better than GA-PI and conventional PI and performs better than or at least competitive with BIA-MPC.

4.4. Experiment IV

In the fourth Experiment, we extend the proposed controller to a three-area interconnected power system, whose schematic diagram is given in Fig. 30 and corresponding system parameters are given Appendix A.4. Here, step load changes are added to area 1 2 and 3: $\Delta P_{L1} = 0.1$pu, $\Delta P_{L2} = 0.08$pu, $\Delta P_{L3} = 0.05$pu. Critical observation of Fig. 31 and Table 14, it demonstrates that the ensemble control performance of proposed CPEO-LMI-PI controller is better than H_∞-LMI control strategy, which indicates that CPEO-LMI-PI controller is more robust against large perturbations. In addition, the proposed control has a simpler structure, which is more appealing from an implementation point of view because the H_∞-LMI controller is of 9th order.

5. Conclusion

In this paper, we have proposed a robust PI controller with its parameters optimized by CPEO embedded by TCH method to handle the constraint called CPEO-LMI-PI control scheme, wherein the LMI technique is applied to describe the H_∞ constraints and *ITAE* taking error performance requirement constraint is employed as another constraint for improving the control performance and dealing with some nonlinear terms. To validate the strong competitiveness, we use four Experiments by comparing with different controllers. Through the experimental comparison results, the following conclusion can be draw:

(1) Compared with CPSO-LMI-PI the proposed CPEO-LMI-PI based LFC has a better control performance on two-area interconnected with GRC and GDB. Additionally, CPEO has faster convergence and

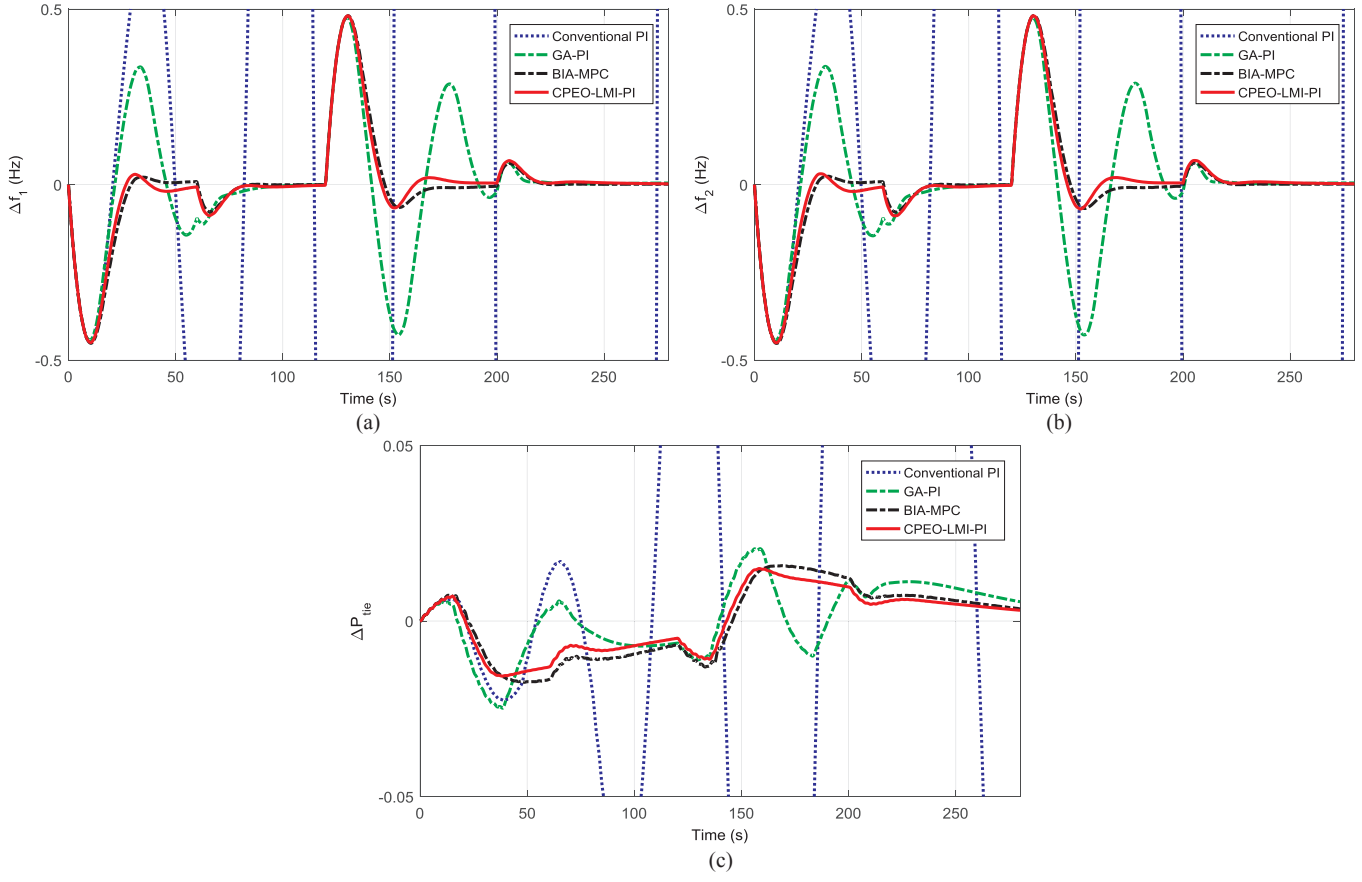

Fig. 29. Comparison of system response subject to Scenario 4 under Experiment III: (a) Δf_1, (b) Δf_2, (c) ΔP_{tie}.

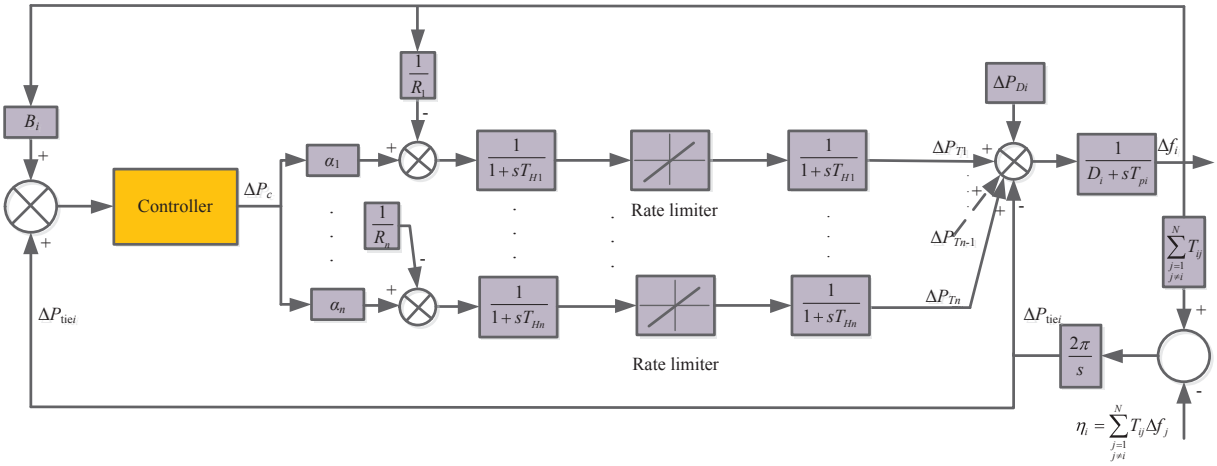

Fig. 30. Three-area interconnected power system under Experiment IV [26].

better global search ability than CPSO algorithm. From the perspective of algorithm design, the proposed CPEO algorithm is simpler than CPSO algorithm, due to its fewer adjustable parameters to be tuned and only mutation operation to be designed.

(2) CPEO-LMI-PI control method outperforms other existing PI controllers (i.e., BFOA-PI [17], GA-PI [17], and conventional PI [17]) for two-area linear interconnected power system under various loading conditions and system parameters changes.

(3) Considering some nonlinear terms (i.e., GRC, GDB, boiler dynamics and time delay) in the two-area interconnected power system, the superiority of the proposed controller is demonstrated by the comparison of GA-PI [30], conventional PI [30] and BIA-MPC [30].

(4) The proposed controller can be extended to a large scale power system. And the experimental comparison results have revealed its effectiveness in dealing with LFC problem of three-area interconnected power system.

Overall, the suggested method can be considered as another novel

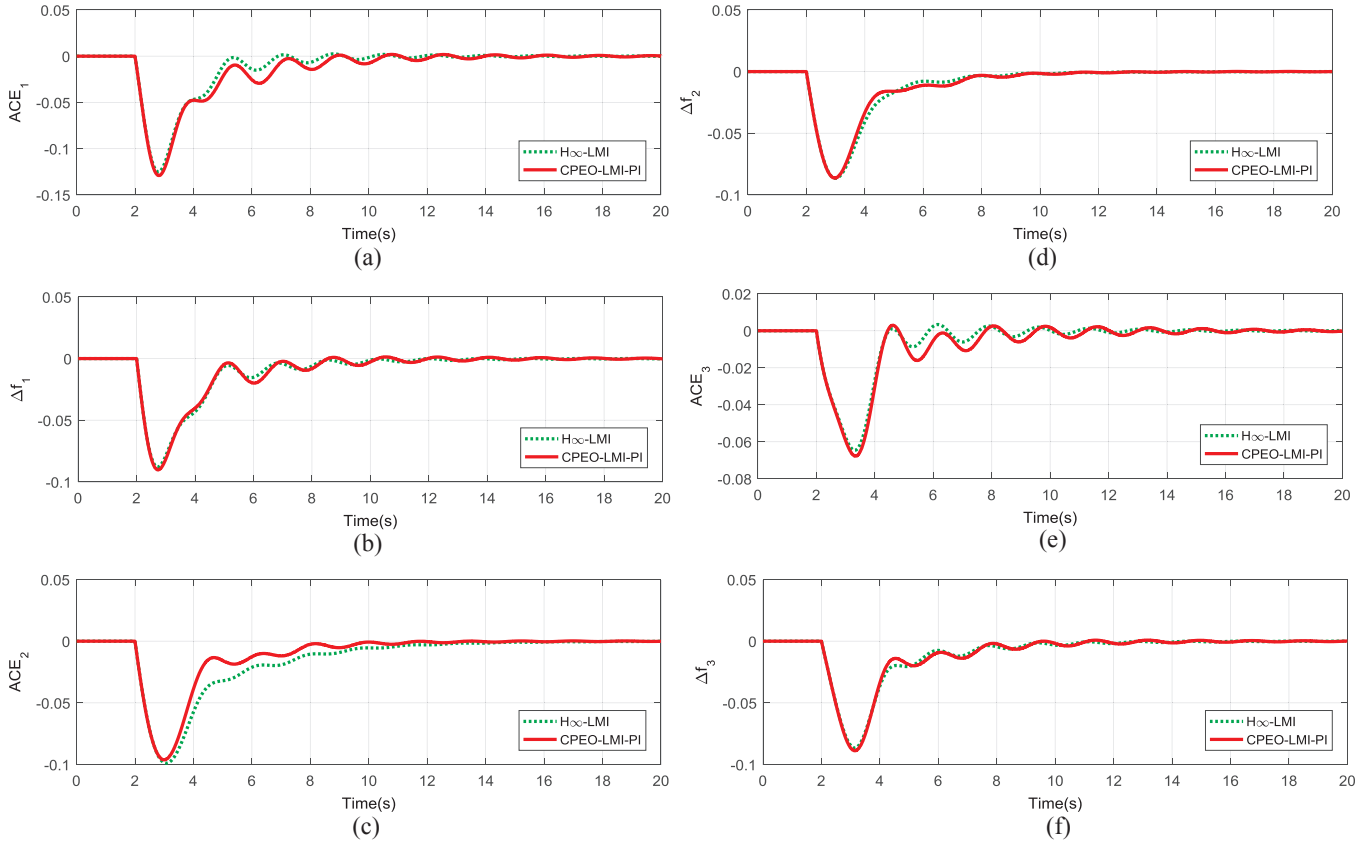

Fig. 31. Comparison of frequency deviation and tie-line power deviation obtained by different controllers for power system under Experiment IV in all the three areas (a) ACE_1, (b) Δf_1, (c) ACE_2, (d) Δf_2, (e) ACE_3, (f) Δf_3.

Table 14
Performance comparison of H_∞-based controller and CPEO-LMI-PI under Experiment VI.

Algorithm	*IAE*	*ITAE*	*ISE*	*ITSE*	*Controller order*
H_∞-LMI	0.7841	3.6324	0.0312	0.1045	9
CPEO-LMI-PI	0.7464	3.4365	0.0308	0.1021	1

promising robust PI controller for LFC problem of interconnected power system with and without nonlinearities to achieve the satisfied responses. Nevertheless, the control behavior of CPEO-LMI-PI may be further improved via a deeper insight into the adjustable parameters by a highly tailored theory. In future, it will be an important subject to design more accurate model of the power system by considering electrical constraints. Also, investigating the load sharing method [52] and application the CPEO-LMI-PI to a more complex system (e.g., varying time delay [51]) are significant topics for future study.

Conflict of interest

There is no conflict of interest.

Acknowledgments

This work was partially supported by Natural Science Foundation of China (Grant No.61573095), and Zhejiang Provincial Natural Science Foundation of China (Nos. LY16F030011 and LZ16E050002).

Appendix A

A.1. Nominal parameters of the two area system under Experiment I are shown below:

$T_1 = 0.6$ s; $T_2 = 5$ s; $T_3 = 32$ s; $Tw = 1$ s; $\lambda_1 = 0.383$pu MW/Hz; $\lambda_2 = 0.425$pu MW/Hz; $T_{p1} = 3.76$ s; $T_{p2} = 20$ s; $K_{p1} = 20$ Hz/p.u. MW; $K_{p2} = 120$ Hz/p.u. MW; $T_r = 10$ s; $T_g = 0.08$ s; $K_r = 0.5$pu MW; $R_1 = 3$ Hz/p.u. MW; $R_2 = 2.4$ Hz/p.u. MW.

For thermal system (area 1): GRC = 0.0017 MW/s; GDB = 0.045 MW/s.

For hydro system (area 2): GRC = 0.045 MW/s for increasing generation and GRC = 0.06 MW/s for decreasing generation; GDB = 0.0002;

A.2. Nominal parameters of the two area system under Experiment II are given as follows:

$\lambda_1 = \lambda_2 = 0.045$pu MW/Hz; $R_1 = R_2 = 2.4$ Hz/p.u.; $T_{g1} = T_{g2} = 0.03$ s; $T_{t1} = T_{t2} = 0.3$ s; $T_{12} = 0.545$pu; $a_{12} = -1$; $K_{ps1} = K_{ps2} = 120$ Hz/p.u. MW; $T_{ps1} = T_{ps2} = 20$ s;

A.3. Nominal parameters of the two area systems under Experiment III are given as follows:

$T_{t1} = 0.3$ s; $T_{g1} = 0.2$ s; $T_{r1} = 10$ s; $K_{r1} = 0.333$; $T_1 = 48.7$ s; $T_2 = 0.513$ s; $T_3 = 10$ s; $T_w = 1$ s; $T_{p1} = 20$ s; $T_{p2} = 13$ s; $K_{p1} = 120$ Hz/p.u. MW; $K_{p2} = 80$ Hz/p.u. MW; $T_{12} = 0.0707$ MW/rad; $a_{12} = -1$; $R_1 = R_2 = 2.4$ Hz/p.u. MW; $\lambda_1 = \lambda_2 = 0.425$pu MW/Hz.

The boiler parameters: $K_1 = 0.85$; $K_2 = 0.095$; $K_3 = 0.92$; $C_b = 200$; $T_f = 10$; $K_{ib} = 0.03$; $T_{ib} = 26$; $T_{rb} = 69$;

For thermal system (area 1): GRC = 0.0017 MW/s; GDB = 0.045 MW/s.

For hydro system (area 2): GRC = 0.045 MW/s for increasing generation and GRC = 0.06 MW/s for decreasing generation; GDB = 0.0002;

A.4. Nominal parameters of the three area systems under Experiment IV are given as follows:

Parameters	Generation companies								
MVA_{base} (1000 MW)	1	2	3	4	5	6	7	8	9
Rate (MW)	1000	800	1000	1100	900	1200	850	1000	1020
D (p.u./Hz)	0.0150	0.0140	0.0150	0.0160	0.0140	0.0140	0.0150	0.0160	0.0150
T_p (p.u.sec)	0.1667	0.1200	0.2000	0.2017	0.1500	0.1960	0.1247	0.1667	0.1870
T_T (sec)	0.4	0.36	0.42	0.44	0.32	0.40	0.30	0.40	0.41
T_H (sec)	0.08	0.06	0.07	0.06	0.06	0.08	0.07	0.07	0.08
R (Hz/p.u.)	3.00	3.00	3.30	2.7273	2.6667	2.50	2.8235	3.00	2.9412
B (p.u./Hz)	0.3438	0.3473	0.3180	0.3827	0.3890	0.4140	0.3692	0.3493	0.3550
α	0.4	0.4	0.2	0.6	0	0.4	0	0.5	0.5
Ramp rateMW/min	8	8	4	12	0	8	0	10	10

References

[1] Shankar R, Pradhan SR, Chatterjee K, Mandal R. A comprehensive state of the art literature survey on LFC mechanism for power systems. Renew Sustain Energy Rev 2017;76:1185–207.
[2] Wu Y, Wei Z, Weng J, Li X, Deng RH. Resonance attacks on load frequency control of smart grids. IEEE Trans Smart Grid 2017. https://doi.org/10.1109/TSG.2017.2661307.
[3] Khooban MH, Niknam T, Shasadeghi M, Dragicevic T, Blaabjerg F. Load frequency control in microgrids based on a stochastic noninteger controller. IEEE Trans Sustain Energy 2018;9(2):853–61.
[4] Khooban MH, Dragicevic T, Blaabjerg F, Delimar M. Shipboard microgrids: a novel approach to load frequency control. IEEE Trans Sustain Energy 2018;9(2):843–52.
[5] Liu X, Zhang Y, Qu B. Robust DMPC for power system load frequency control with state-error. Mobile Netw Appl 2017;22(3):405–17.
[6] Mohamed TH, Bevrani H, Hassan AA, Hiyama T. Decentralized model predictive based load frequency control in an interconnected power system. Energy Convers Manag 2011;52(2):1208–14.
[7] Liu X, Zhang Y, Lee KY. Coordinated distributed MPC for load frequency control of power system with wind farms. IEEE Trans Ind Electron 2017;64(6):5140–50.
[8] Liu X, Kong X, Lee KY. Distributed model predictive control for load frequency control with dynamic fuzzy valve position modelling for hydro–thermal power system. IET Control Theory Appl 2016;10(14):1653–64.
[9] Liu X, Zhang Y, Lee KY. Robust distributed MPC for load frequency control of uncertain power systems. Control Eng Pract 2016;56:136–47.
[10] Bevrani H, Feizi MR, Ataee S. Robust frequency control in an islanded microgrid: H_∞ and μ-synthesis approaches. IEEE Trans Smart Grid 2016;7(2):706–17.
[11] Mahto T, Mukherjee V. A novel scaling factor based fuzzy logic controller for frequency control of an isolated hybrid power system. Energy 2017;130:339–50.
[12] Modirkhazeni A, Almasi ON, Khooban MH. Improved frequency dynamic in isolated hybrid power system using an intelligent method. Int J Electr Power Energy Syst 2016;78:225–38.
[13] Bevrani H, Daneshmand PR. Fuzzy logic-based load-frequency control concerning high penetration of wind turbines. IEEE Syst J 2012;6(1):173–80.
[14] Khooban MH. Secondary load frequency control of time-delay stand-alone microgrids with electric vehicles. IEEE Trans Ind Electron 2018;65(9):7416–22.
[15] Singh VP, Kishor N, Samuel P. Improved load frequency control of power system using LMI based PID approach. J Franklin Inst 2017;354(15):6805–30.
[16] Gholamrezaie V, Dozein MG, Monsef H, Wu B. An optimal frequency control

method through a dynamic load frequency control (LFC) model incorporating wind farm. IEEE Syst J 2018;12(1):392–401.
[17] Ali ES, Abd-Elazim SM. Bacteria foraging optimization algorithm based load frequency controller for interconnected power system. Int J Electr Power Energy Syst 2011;33(3):633–8.
[18] Mohanty B, Panda S, Hota PK. Controller parameters tuning of differential evolution algorithm and its application to load frequency control of multisource power system. Int J Electr Power Energy Syst 2014;54:77–85.
[19] Khooban MH, Niknam T, Blaabjerg F, Dragicevic T. A new load frequency control strategy for micro-grids with considering electrical vehicles. Electr Power Syst Res 2017;143:585–98.
[20] Abd-Elaziz AY, Ali ES. Cuckoo search algorithm based load frequency controller design for nonlinear interconnected power system. Int J Electr Power Energy Syst 2015;73:632–43.
[21] Abd-Elazim SM, Ali ES. Load frequency controller design via BAT algorithm for nonlinear interconnected power system. Int J Electr Power Energy Syst 2016;77:166–77.
[22] Abd-Elazim SM, Ali ES. Load frequency controller design of a two-area system composing of PV grid and thermal generator via firefly algorithm. Neural Comput Appl 2016:1–10.
[23] Khalghani MR, Khooban H, Mahboubi-Moghaddam E, Vafamand N, Goodarzi M. A self-tuning load frequency control strategy for microgrids: Human brain emotional learning. Int J Electr Power Energy Syst 2016;75:311–9.
[24] Khooban MH, Niknam T, Blaabjerg F, Davari P, Dragicevic T. A robust adaptive load frequency control for micro-grids. ISA Trans 2016;65:220–9.
[25] Kumar LVS, Kumar GVN, Madichetty S. Pattern search algorithm based automatic online parameter estimation for AGC with effects of wind power. Int J Electr Power Energy Syst 2017;84:135–42.
[26] Rerkpreedapong D, Hasanovic A, Feliachi A. Robust load frequency control using genetic algorithms and linear matrix inequalities. IEEE Trans Power Syst 2003;2(18):855–61.
[27] Selvaraju RK, Somaskandan G. Impact of energy storage units on load frequency control of deregulated power systems. Energy 2016;97:214–28.
[28] Pandey SK, Mohanty SR, Kishor N, Catalao JPS. Frequency regulation in hybrid power systems using particle swarm optimization and linear matrix inequalities based robust controller design. Int J Electr Power Energy Syst 2014;63:887–900.
[29] Velusami S, Chidambaram IA. Decentralized biased dual mode controllers for load frequency control of interconnected power systems considering GDB and GRC nonlinearities. Energy Convers Manag 2007;48:1691–702.
[30] Elsisi M, Soliman M, Aboelela MAS, Mansour W. Bat inspired algorithm based optimal design of model predictive load frequency control. Int J Electr Power Energy Syst 2016;83:426–33.
[31] Tan W, Chang S, Zhou R. Load frequency control of power systems with non-linearities. IET Gener Transm Distrib 2017;11(17):4307–13.
[32] Kadhar KMA, Baskar S. Covariance matrix adaptation evolution strategy based design of fixed structure robust H∞ loop shaping controller. Appl Soft Comput 2015;34:337–48.
[33] Zhao SZ, Iruthayarajan MW, Baskar S, Suganthan PN. Multi-objective robust PID controller tuning using two lbests multi-objective particle swarm optimization. Inf Sci 2011;181(16):3323–35.
[34] Boettcher S, Percus AG. Optimization with extremal dynamics. Phys Rev Lett 2001;86(23):5211–4.
[35] Boettcher S, Percus AG. Nature's way of optimizing. Artif Intell 2000;119:275–86.
[36] Bak P, Sneppen K. Punctuated equilibrium and criticality in a simple model of evolution. Phys Rev Lett 1993;71:4083.
[37] Li L, Lu K, Zeng G, Wu L, Chen M. A novel real-coded population-based extremal optimization algorithm with polynomial mutation: A non-parametric statistical study on continuous optimization problems. Neurocomputing 2016;174:577–87.
[38] Chen M, Lu Y, Yang G. Multiobjective optimization using population-based extremal optimization. Neural Comput Appl 2008;17(2):101–9.
[39] Zeng G, Chen J, Li L, Chen M, Wu L, Dai Y. An improved multi-objective population-based extremal optimization algorithm with polynomial mutation. Inf Sci 2016;330:49–73.
[40] Lu Y, Chen Y, Chen M, Chen P, Zeng G. Extremal optimization: fundamentals, algorithms, and applications. Boca Raton, FL, USA: CRC Press & Chemical Industry Press; 2016.
[41] Zeng G, Chen J, Chen M, Dai Y, Li L, Lu K, et al. Design of multivariable PID controllers using real-coded population-based extremal optimization. Neurocomputing 2015;151:1343–53.
[42] Zeng G, Chen J, Dai Y, Li L, Zheng C, Chen M. Design of fractional order PID controller for automatic regulator voltage system based on multi-objective extremal optimization. Neurocomputing 2015;160:173–84.
[43] Wang H, Zeng G, Dai Y, Bi D, Sun J, Xie X. Design of a fractional order frequency PID controller for an islanded microgrid: a multi-objective extremal optimization method. Energies 2017;10(10):1502.
[44] Lu K, Zhou W, Zeng G, Du W. Design of PID controller based on a self-adaptive statespace predictive functional control using extremal optimization method. J Franklin Inst 2018;355:2197–220.
[45] Falco ID, Laskowski E, Olejnik R, Scafuri U, Tarantino E, Tudruj M. Extremal optimization applied to load balancing in execution of distributed programs. Appl Soft Comput 2015;30:501–13.
[46] Deb K, Pratap A, Agarwal S, Meyarivan T. A fast and elitist multiobjective genetic algorithm: NSGA-II. IEEE Trans Evol Comput 2002;6:182–97.
[47] Gahinet P, Nemirovski A, Laub AJ, Chilali M. LMI control toolbox. The MathWorks, Inc; 2014.
[48] Ali ES. Optimization of power system stabilizers using BAT search algorithm. Int J Electr Power Energy Syst 2014;6(1):683–90.
[49] Tang PH, Tseng MH. Adaptive directed mutation for real-coded genetic algorithms. Appl Soft Comput 2013;13:600–14.
[50] Ho SY, Shu LS, Chen JH. Intelligent evolutionary algorithms for large parameter optimization problems. IEEE Trans Evol Comput 2004;8(6):522–41.
[51] Jiang L, Yao W, Wu QH, Wen JY, Cheng SJ. Delay-dependent stability for load frequency control with constant and time-varying delays. IEEE Trans Power Syst 2012;27(2):932–41.
[52] Dehghani M, Khooban MH, Niknam T, Rafiei SMR. Time-varying sliding mode control strategy for multibus low-voltage microgrids with parallel connected renewable power sources in islanding mode. J Energ Eng 2016;142(4):05016002.